

# 1 **Detecting the resilience of soil moisture dynamics to drought** 2 **periods as function of soil type and climatic region**

3 Nedal Aqel<sup>1</sup>, Jannis Groh<sup>2,3</sup>, Lutz Weihermüller<sup>2</sup>, Ralf Gründling<sup>4</sup>, Andrea Carminati<sup>1</sup>, Peter  
4 Lehmann<sup>1</sup>

5 <sup>1</sup>Physics of Soils and Terrestrial Ecosystems, ETH Zurich, Zurich, Switzerland

6 <sup>2</sup>Institute of Bio- and Geoscience IBG-3: Agrosphere, Forschungszentrum Jülich GmbH, Jülich, Germany

7 <sup>3</sup>Biogeochemistry and Gas Fluxes, Leibniz Institute for Agricultural and Landscape Research (ZALF),  
8 Müncheberg, Germany

9 <sup>4</sup>Department of Soil System Science, Helmholtz-Zentrum für Umweltforschung GmbH – UFZ, Halle, Germany

10 \*Corresponding author, [nedal.aqel@usys.ethz.ch](mailto:nedal.aqel@usys.ethz.ch), Universitätstrasse 16, 8092 Zurich, Switzerland

## 11 **Abstract**

12 Abrupt changes in climatic conditions and land management can cause permanent shifts in soil  
13 hydraulic response to climatic inputs, impacting soil functions and established soil–climate interactions.  
14 To quantify the resilience of soil water content dynamics after abrupt changes in environmental  
15 conditions, we present a model framework combining a neural network with seasonal trend analysis  
16 (STL). Using data from a series of lysimeter from the TERrestrial ENvironmental Observatories  
17 (TERENO) - SOILCan lysimeter network, we identified changes in the response of soil water content  
18 after an extremely hot and dry summer in Germany in the year 2018. The model incorporates  
19 meteorological variables decomposed into seasonal and long-term components along with a categorical  
20 indicator of current moisture conditions. It is trained on data from a reference site with stable soil water  
21 content response and applied to lysimeters from multiple origins exposed to contrasting climates. By  
22 analysing annual residual patterns—particularly mean bias over time—soil water content state  
23 dynamics is classified as ‘stable’, ‘resilient’, or ‘changed’, reflecting whether the system maintains,  
24 recovers, or diverges from its original state. We found that soils preserve the response function to  
25 environmental forcing under typical conditions but exhibit changes in hydraulic behaviour when  
26 relocated to new environments, even when soil texture remains constant. The proposed method offers  
27 a scalable and non-invasive tool for tracking changes in the response of soil water content to climatic  
28 change and provides early indicators of changes in essential soil functions and soil health status.

## 29 1. Introduction

30 Soil water content plays a fundamental role in hydrological processes and land–atmosphere interactions,  
31 governing the exchange of water and energy at the Earth’s surface (Seneviratne et al., 2010; Sun et al.,  
32 2025). It regulates key hydrological functions, including infiltration, runoff generation,  
33 evapotranspiration, and groundwater recharge. Through these processes, soil water content influences  
34 water availability, ecosystem productivity, and climatic conditions across local to global scales (Bogena  
35 et al., 2015; Fatichi et al., 2020). Soil water content status and related soil environmental conditions  
36 change with short- and long-term atmospheric processes. This response of soil water content to  
37 atmospheric conditions, which we define as ‘soil water content response function’, determines, for  
38 example, if anaerobic conditions are inhibited after heavy rainfall (by fast percolation to deeper soil  
39 layers) and if enough water remains available after dry periods for plant growth, temperature regulation,  
40 and chemical reactions. In short, the soil water content response function is an indicator of near-surface  
41 hydraulic functioning and land–atmosphere exchange processes, which are relevant for several soil  
42 health–related processes such as infiltration efficiency, surface aeration, and runoff generation. This  
43 response function is shaped by soil formation processes and reflects adaptation to the dominant climatic  
44 conditions (Kuzyakov and Zamanian, 2019; Sainju et al., 2022). Accordingly, a change in the response  
45 function after extreme climatic events is likely to imply a change in soil health.

46 In the core of this study is the question how changes in the soil water content response function, and  
47 thus in soil properties and health, can be detected. The standard approach to determine the response  
48 function is to apply physically based models, for example by inverse modelling of soil water content  
49 dynamics under varying boundary conditions (Šimůnek et al., 2016). These models require detailed  
50 knowledge of soil hydraulic properties and extensive calibration, limiting their generalization beyond  
51 the spatial scale and the local conditions used in the calibration process (Lehmann et al., 2020; O. &  
52 Orth, 2021). Additionally, soil hydraulic parameters for physically based models are usually obtained  
53 through soil sampling or sensor installation, both of which disturb the soil structure, limiting the  
54 feasibility of repeated measurements for long-term time-series analysis. Moreover, these models  
55 typically assume static soil characteristics, failing to adequately represent structural changes in soil

56 properties—such as compaction, degradation, or organic matter loss—that can substantially alter  
57 hydraulic behaviour over time (Faticchi et al., 2020; Melsen & Guse, 2021; Wankmüller et al., 2024).  
58 Most of the models also neglect or oversimplify the hysteretic nature of the soil water retention curve,  
59 as well as seasonal changes in soil hydraulic properties that can substantially alter infiltration, drainage,  
60 and plant water availability (Aqel et al., 2024; Hannes et al., 2016; Herbrich & Gerke, 2017). Therefore,  
61 we used a non-invasive approach based on neural networks as discussed below.

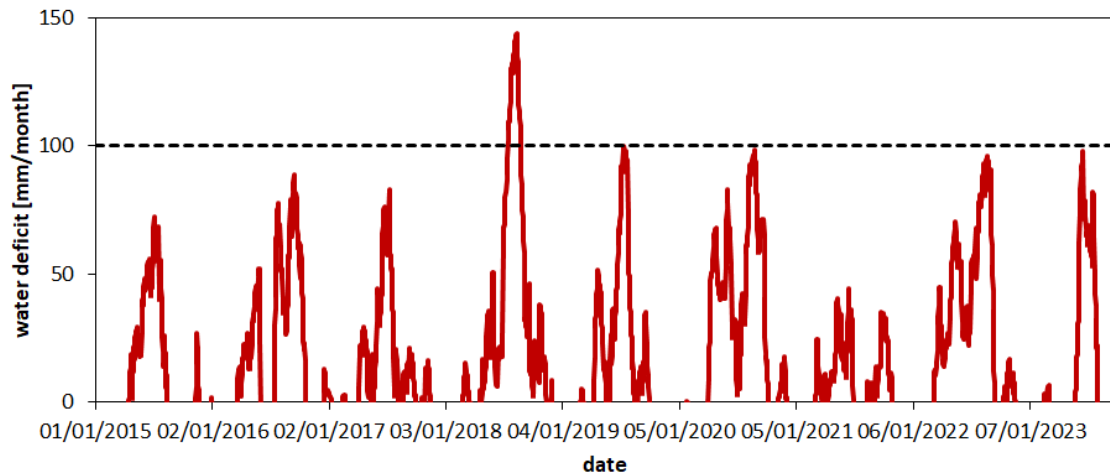
62 In recent years, artificial intelligence (AI), particularly neural networks, has emerged as a promising  
63 alternative for modelling complex hydrological processes (Reichstein et al., 2019). These data-driven  
64 models have demonstrated the capacity to learn nonlinear relationships directly from observational  
65 datasets without relying heavily on explicit physical equations (Kratzert et al., 2019; Mosavi et al.,  
66 2018; Shen et al., 2018). Within soil hydrology, neural networks have been used to characterise  
67 hysteretic soil–water behaviour from training data, improving the representation of wetting–drying  
68 cycles without explicit hysteresis parameterisation (Aqel et al., 2024). They have also been applied to  
69 soil-moisture time-series modelling using Long Short-Term Memory (LSTM) networks with recurrent  
70 architectures suited to capture long-range temporal dependencies (Liu et al., 2023; O. & Orth, 2021).  
71 Across diverse hydro-climatic regimes, LSTM have been shown to effectively learn nonlinear  
72 relationships between climatic inputs and soil water content, often matching or surpassing traditional  
73 physically based approaches and demonstrating strong generalisation (Kratzert et al., 2019; J. Liu et al.,  
74 2022, 2023; O. & Orth, 2021).

75 Independent of the chosen modelling approach, these models ignore that the soil water content response  
76 function (i.e., the variations in soil water content following changes in atmospheric conditions) can  
77 change at a larger time scale. Experimental studies have shown that extreme events such as drought can  
78 induce persistent shifts in soil water content dynamics, potentially leading to alternative stable states  
79 see Robinson et al., 2016, Quintana et al., 2023 and the section on illustrative examples in Robinson et  
80 al., 2019). Moreover, changes in land use—such as forest conversion to agriculture or bare land—alter  
81 soil hydraulic properties, with effects on infiltration, water retention, and saturated hydraulic  
82 conductivity (Fu et al., 2021; Robinson et al., 2022). Considering that soil texture (particle-size

83 distribution) remains constant at time scales of decades, the changes in the response function are likely  
84 to be related to changes in soil structure and associated hydraulic properties driven by structural  
85 reorganization, wettability effects, root activity, or land-use changes rather than to textural change.

86 Soil systems are subject to temporal change, yet models are often trained on historical datasets without  
87 evaluating whether the system dynamics remain stable throughout the training period (Montanari et al.,  
88 2013; Vaze et al., 2010). As a result, models may be applied to prediction settings where underlying  
89 soil–climate interactions differ from those on which the model was trained. For example, a recent study  
90 comparing different crop models using the TERENO-SOILCan set-up showed that predicting  
91 agronomic and environmental variables under different climatic conditions to those represented in the  
92 training datasets resulted in significant discrepancies between simulations and observations (Groh et  
93 al., 2022). This underscores the critical need to assess whether site-specific representations of soil–  
94 water behaviour remain valid over time (Hrachowitz et al., 2013) and highlight the need for more  
95 adaptable modelling approaches under evolving environmental conditions (Blöschl et al., 2019; Milly  
96 et al., 2008). A recent modelling framework by Jarvis et al. (2024) takes a major conceptual step forward  
97 by explicitly representing soil-structure dynamics and their feedback on hydraulic behaviour. However,  
98 as the authors emphasize, such process-based models still depend on detailed observational data to  
99 constrain temporal changes in structure and hydraulic properties.

100 To address this gap, the present study introduces a framework based on neural networks and seasonal  
101 trend decomposition. This framework is applied to quantify changes in the soil response function  
102 following the 2018 summer drought, a Europe-wide extreme event. During this period, total  
103 precipitation in central Europe fell to the lowest percentiles relative to the 1976–2005 reference  
104 distribution. In Germany, the summer of 2018 was characterised by one of the warmest years on record  
105 and the lowest precipitation since 1881 (Xoplaki et al., 2025). The response of soil water content on  
106 this drought will be analysed with a set of lysimeters. As shown in Fig. 1 for one of the study sites, the  
107 monthly water deficit (potential evapotranspiration minus precipitation) peaked in summer 2018  
108 indicating the strong drought in this period.



109 **Figure 1** Variations in climatic conditions at Selhausen (SE) expressed as difference between potential  
 110 evapotranspiration (PET) and precipitation (P) cumulated over the precedent 30 days (one month). The extreme  
 111 summer 2018 is manifested by a maximum monthly deficit of ~150 mm. Details on the calculation of PET are  
 112 provided in section 2.1.1.  
 113

114 The general objective of this study is to introduce a model framework to quantitatively detect changes  
 115 in the soil water content response function and to classify the response as “stable”, “resilient”, or  
 116 “changed”. These terms are used here as operational classes describing the temporal behaviour of the  
 117 response function, rather than as formal system-level properties or metrics as defined in ecological and  
 118 complex systems theory. In that literature, resilience is commonly understood as a system property  
 119 reflecting the capacity to absorb disturbance and recover, while stability refers to the tendency of system  
 120 dynamics to remain close to a reference state or equilibrium (Holling, 1973). Resilience is often  
 121 discussed in relation to both resistance to perturbation and the subsequent recovery toward pre-  
 122 established levels. In the context of this study, “stable” denotes the validity of a single response function  
 123 throughout the entire monitoring period. “Resilient” denotes a temporary deviation from this response  
 124 function following an extreme event (summer 2018), followed by a return to the pre-event response  
 125 within the observation window. In the third case, denoted here as “changed”, the response function at  
 126 the end of the observation period remains distinct from the pre-2018 reference response. Whether such  
 127 a change represents a persistent transition to an alternative response regime or a transient deviation with  
 128 delayed recovery cannot be determined based on the available time series.

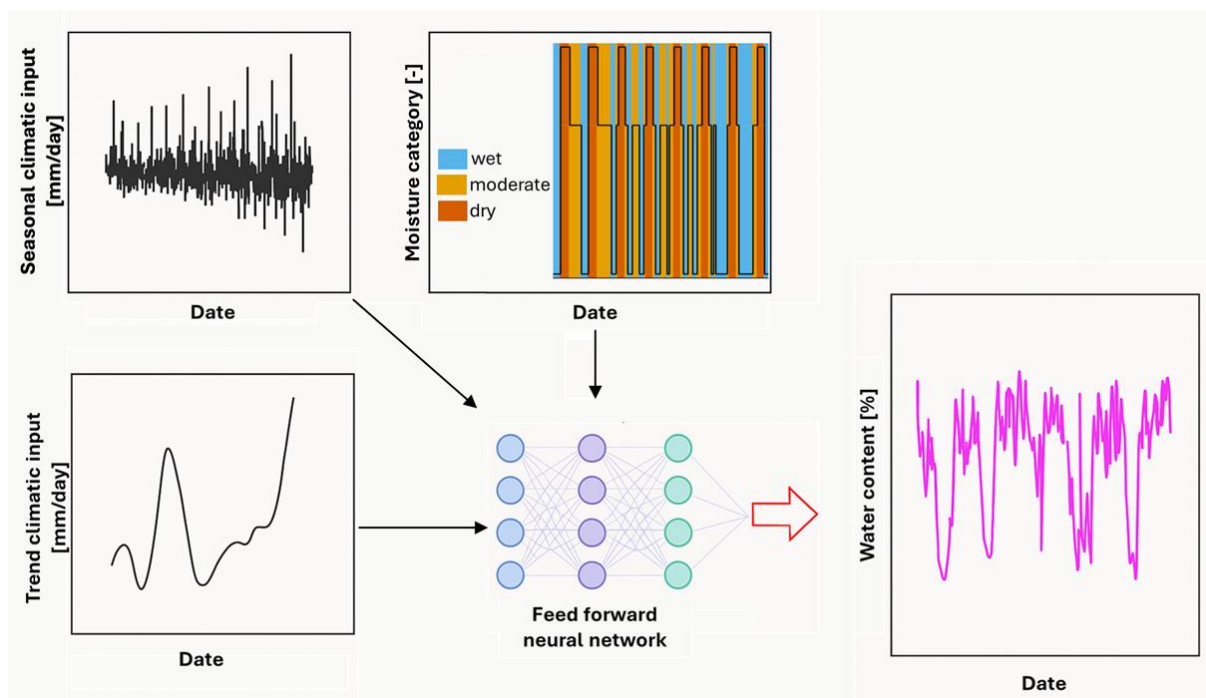
129

130

131 In principle, it would be possible to develop a quantitative framework to detect changes in the response  
132 function exclusively based on experimental data of time series (without modelling), for example by the  
133 application of wavelet analysis (Ehrhardt et al., 2025). In this study, we adopt a predictive modelling  
134 approach in which deviations between observed and simulated soil water content over time are used to  
135 identify changes in the soil–climate response function. While the model also produces predictions of  
136 soil water content, prediction accuracy is not the primary objective; instead, model–data deviations are  
137 used to detect temporal drift in soil water response behaviour. The overall level of dynamic agreement  
138 is summarized using Nash–Sutcliffe efficiency, while the detection and classification of changes rely  
139 on the temporal evolution of mean bias, as described in Section 2.5.

## 140 2. Material and Methods

141 We developed a data-driven modelling framework that combines time-series decomposition of climatic  
142 inputs with a feed-forward neural network to predict the daily soil water content (Fig. 2).



143 **Figure 2** Schematic overview of the modelling framework for daily soil water content prediction. Input features  
144 include the analysis of a climatic variable (top left), its long-term trend component (bottom left), and the  
145 categorical soil water content state ('wet', 'moderate', 'dry'; top middle). These features, derived from observed  
146 data, are used to train a feed-forward neural network (centre), which outputs daily predictions of volumetric  
147

148 *water content (right). The model thus captures temporal soil water content dynamics based on structured climate*  
149 *signals and categorical conditions.*

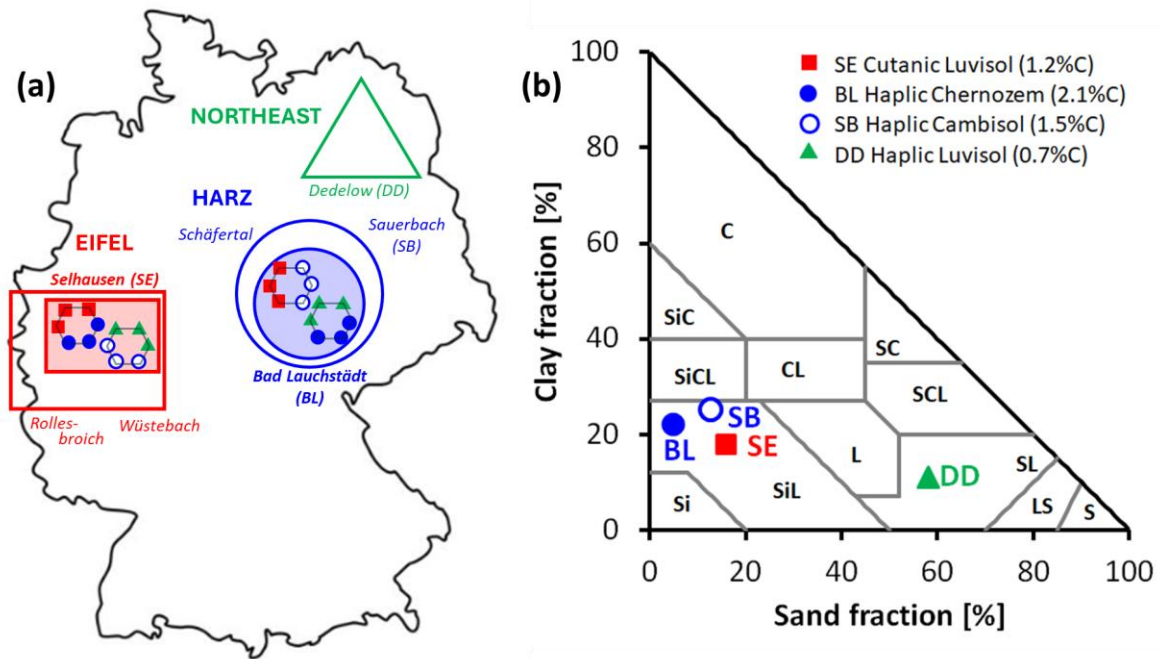
150 The approach explicitly incorporates precipitation (P), potential evapotranspiration (PET), and their  
151 difference (climatic water balance) as primary inputs. Each of these climate drivers was decomposed  
152 into seasonal variations and long-term trend components using Seasonal-Trend decomposition (STL)  
153 and was included as a separate feature in the model (Boergens et al., 2024; Cleveland et al., 1990). The  
154 daily climatic water balance (WB) was included to reflect the net difference between P and PET, serving  
155 as a proxy for wetting or drying conditions. Positive values indicate potential moisture accumulation  
156 (e.g., during rainfall-dominated periods), while negative values reflect high evaporative demand and  
157 drying conditions (e.g., during hot, dry spells). Including the WB helps the model to distinguish humid  
158 periods from dry ones. By providing WB alongside P and PET, the model can learn both the individual  
159 and combined effects of precipitation and evaporative demand on soil water content dynamics (Brocca  
160 et al., 2010; Uber et al., 2018). For example, it can infer that 10 mm of P during a high-PET summer  
161 day (low positive or negative WB) is less likely to increase soil water content than the same P on a cool,  
162 low-PET day (high positive WB).

163 The input features also included a categorical moisture class (type) that reflects the expected current  
164 soil water condition ('wet', 'moderate', 'dry'). This design reflects the understanding that changes in  
165 climate - such as shifts in rainfall and evaporative demand - substantially affect soil water availability  
166 and fluxes (Vereecken et al., 2022). The methodology is detailed in the following sections, which  
167 consists of five key steps: selecting study sites and datasets collected in contrasting hydro-climatic  
168 conditions (subsection 2.1), preprocessing the data and extracting meaningful signals features including  
169 STL (subsection 2.2), constructing and training a neural network model on a reference dataset  
170 (subsection 2.3), generating soil water content predictions for independent (non-training) sites using the  
171 trained model (subsection 2.4), evaluating the model's performance with statistical metrics (subsection  
172 2.5), and physical consistency checks (subsection 2.6).

## 173 2.1 Study Sites and Data Selection

### 174 2.1.1 Lysimeter Network TERENO SOILCan

175 The study was conducted using lysimeter data from the TERENO-SOILCan lysimeter network in  
176 Germany (Pütz et al., 2016) with a focus on two locations: Bad Lauchstädt (BL) and Selhausen (SE)  
177 (Fig. 3). These sites were selected for their contrasting climatic regimes and the specific set-up of  
178 lysimeters, providing a natural experiment on how climate variability influences soil hydrological  
179 behaviour for a variety of soils. The TERENO-SOILCan lysimeters were moved between and within  
180 observatories according to a modified space-for-time approach, to expose them to different climates  
181 (Groh et al. 2020). This allows us to compare the ecosystem response of the same soil, but under  
182 different climatic conditions. Selhausen is characterized by a humid, Atlantic-influenced climate  
183 (annual precipitation around 720 mm and mean air temperature around 10 °C), whereas Bad Lauchstädt  
184 represents a drier, more continental climate (annual precipitation roughly 487 mm and mean air  
185 temperature approximately 8.8 °C); both climate descriptions were based on Pütz et al. (2016). Long-  
186 term observations confirmed that Bad Lauchstädt experiences significantly lower rainfall and higher  
187 evaporative demand than Selhausen, yielding a higher aridity index (ratio of potential  
188 evapotranspiration to precipitation) and more pronounced dry spells in the growing season. By  
189 including both, a wetter site (Selhausen) and a drier site (Bad Lauchstädt), the model is evaluated under  
190 distinctly different moisture regimes, which is critical for testing the generality of the approach and to  
191 separate between climatic and soil type effects. For each lysimeter station (Bad Lauchstädt and  
192 Selhausen), 12 lysimeters (1 m<sup>2</sup> surface area, 1.5 m depth) arranged in hexagons with 6 lysimeters  
193 around a service well were included in the analysis to monitor soil water content along with  
194 meteorological variables. In this study, lysimeters were not used for drainage or storage estimates, but  
195 rather as instruments providing long-term, high-resolution time series of soil water content and matric  
196 potential under field conditions. The lysimeters contain undisturbed soil columns collected at four  
197 different locations (see Fig. 3a), each with three replicates (Pütz et al., 2016) and were managed as  
198 arable land under crop rotation. Note that all lysimeters were collected in the field and transported to  
199 the lysimeter station (Pütz et al., 2016) such that no differences regarding packing and boundary effect  
200 can be expected. While fertilization practices differed regionally until spring 2019, the overall  
201 management concept was comparable, ensuring that differences in water dynamics can be attributed to  
202 changes in the climate and soil rather than the management (Pütz et al., 2016).



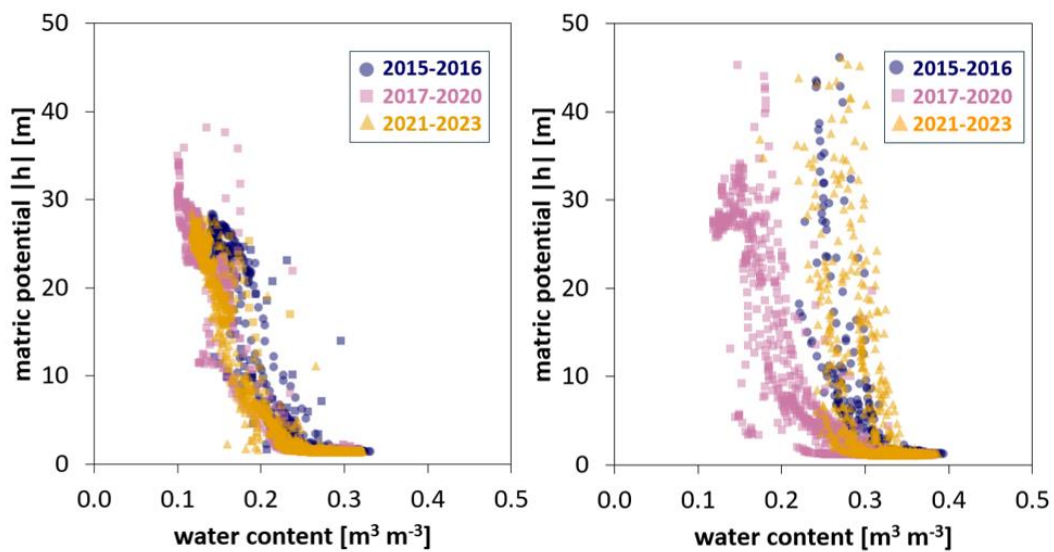
203  
 204 **Figure 3** Overview of the study area with site locations, topsoil texture, and soil origin. (a) The TERENO-  
 205 SOILCan network contains lysimeters from four climatic regions (different symbols and colours in map). Our  
 206 analysis focuses on the TERENO–SOILCan sites Selhausen (SE) and Bad Lauchstädt (BL), located in the  
 207 Eifel/lower rhine valley and Harz/central German lowland observatory of TERENO, respectively, because at both  
 208 sites lysimeter clusters were built (represented by shaded areas and hexagons), collecting large soil columns from  
 209 four distinct source regions (i.e., Dedelow (DD), Bad Lauchstädt (BL), Sauerbach (SB), and Selhausen (SE)). (b)  
 210 The analysed soil horizons (10 cm depth) cover two textural classes, shown in the USDA soil texture triangle,  
 211 assigned to four different soil types and a range of soil organic carbon contents (SOC) (numbers in the legend).

212 To investigate the effects of climate on soil water dynamics, daily time series of precipitation (P),  
 213 potential evapotranspiration (PET), matric potential, and volumetric soil water content (used as the  
 214 target variable) were compiled. Precipitation at Selhausen was measured at the on-site SOILCan  
 215 weather station, while for Bad Lauchstädt it was taken from the nearest long-term monitoring station  
 216 operated by the Deutscher Wetterdienst (Leipzig/Halle, ID 2932; DWD Climate Data Center, 2025).  
 217 PET was calculated with the FAO-56 Penman–Monteith model (Allen et al., 2006), using measured  
 218 meteorological variables (air temperature, air pressure, relative humidity, radiation, and wind speed)  
 219 according to SOILCan protocols (Pütz et al., 2016; Groh et al., 2020). In this context, the reference  
 220 evapotranspiration (ET<sub>o</sub>) calculated with the Penman–Monteith model for a clipped grass surface  
 221 (FAO-56) is used as a proxy for potential evapotranspiration (PET), representing the site-independent  
 222 atmospheric evaporative demand. Soil matric potential was measured using MPS-1 sensors (Decagon  
 223 Devices Inc., Pullman, WA, USA), and volumetric soil water content was measured with time-domain

224 reflectometry probes (CS610, Campbell Scientific, North Logan, UT, USA). The observational record  
225 spans the period from 2014 to 2023 and includes measurements taken at a depth of 10 cm (deeper soil  
226 layers were not analysed; Pütz et al., 2016).

### 227 2.1.2 Definition of Reference Site for Model Framework

228 For model development, a single lysimeter moved from Dedelow to the Bad Lauchstädt lysimeter  
229 station (see Fig. 3a and 3b) was selected as the training dataset. This lysimeter was chosen due to its  
230 stable soil water content dynamics and minimal temporal drift in water retention properties over the  
231 observation period (see Fig. 4a). This lysimeter served as the reference dataset for developing the  
232 predictive model because it allows the definition of soil water content response function for the seasonal  
233 climatic conditions. The 23 remaining lysimeters at the Bad Lauchstädt and Selhausen site were used  
234 as independent test datasets (a contrasting example is shown in Fig. 4b) to evaluate model generalization  
235 and detect potential shifts in soil hydraulic behaviour across sites and years.



236 **Figure 4** Soil water retention curves using data collected between 2015 and 2023 at 10 cm depth. Matric potential  
237 is plotted against volumetric water content, with data colour-coded by period: 2015–2016 (blue), 2017–2020  
238 (green), and 2021–2023 (red). (a) Training lysimeter (moved from Dedelow to Bad Lauchstädt). (b) Test lysimeter  
239 (original soil from Selhausen in lysimeter station at Selhausen).  
240

## 241 2.2 Data Preprocessing and Feature Engineering

242 All raw data were aggregated or resampled to a daily time step to support time-series analysis and  
243 modelling. Any misaligned or duplicated timestamps were corrected to ensure consistency.

244 Measurements before the year 2015 were excluded from both sites to allow sensor settlement after  
245 installation.

### 246 *2.2.1 Seasonal-Trend decomposition*

247 To provide the model with structured representations of climate variability, each climatic time series  
248 was decomposed into additive components using STL based on LOESS with LOESS as acronym for  
249 ‘Locally Estimated Scatterplot Smoothing’ (Cleveland et al., 1990). STL is a non-parametric method  
250 that separates a time series into three interpretable parts: a seasonal component representing repeating  
251 seasonal patterns (such as wetting and drying cycles), a trend component capturing gradual long-term  
252 changes (such as climate shifts), and a residual component containing short-term irregularities and high-  
253 frequency noise (Cleveland et al., 1990). This decomposition was applied independently to the P, PET,  
254 and WB time series. Only the seasonal and trend components were retained as input features, as they  
255 contain meaningful patterns relevant to soil water content dynamics. The residual component, which  
256 lacks systematic structure, was excluded from further analysis. STL was configured with a cycle length  
257 of 180 days, representing the semi-annual wet–dry phases at the study sites. A LOESS smoother with  
258 a 90-day window was then applied to the de-seasonalized series to extract the trend component. This  
259 configuration was chosen to capture gradual, long-term changes in the climatic variables while reducing  
260 short-term fluctuations. Note, that near the ends of the time series the absence of future values causes  
261 the smoothing window to become asymmetric. As a result, the estimated trend becomes more sensitive  
262 to recent variability. This limitation does not affect the outcome of the analysis, as both the input  
263 features and the target variable (water content) are equally influenced by it. Each of the extracted  
264 seasonal and trend components from P, PET, and WB was included as input to the neural network  
265 alongside the original raw values. This allowed the model to learn structured seasonal behaviour—such  
266 as distinguishing the rising phase of spring wetting up of the soil profile from the declining phase of a  
267 summer dry-down—and to account for long-term shifts, such as gradual drying or changes in mean  
268 climate conditions.

### 269 *2.2.2 Wetness classification*

270 In addition to the continuous climate-related features, a categorical input was included to describe the  
271 soil's moisture condition as either 'dry', 'moderate', or 'wet'. These categories were defined using the  
272 soil water content time series from the training site, with thresholds based on quantiles of the full  
273 distribution. Specifically, values below the 30<sup>th</sup> percentile were labelled as 'dry', between the 30<sup>th</sup> and  
274 70<sup>th</sup> percentiles as 'moderate', and above the 70<sup>th</sup> percentile as 'wet'. These categories were then  
275 encoded numerically prior to modelling, using values of 30 for 'dry', 20 for 'moderate', and 1 for 'wet'.  
276 This encoding allowed the categorical feature to be treated as an ordinal variable and integrated into the  
277 neural network input layer alongside the other features. The thresholds were selected to provide clear  
278 regime separation while ensuring sufficient observations per class for robust model training.

279 There are two reasons to include this feature. Firstly, the soil's current moisture condition can strongly  
280 influence its response to P and PET (Western & Grayson, 1998). For example, under dry conditions,  
281 more water can be absorbed by the soil due to its high storage capacity. In contrast, when soils are  
282 already wet or near saturation, infiltration capacity is reduced, and additional rainfall is more likely to  
283 result in runoff (Tromp-van Meerveld & McDonnell, 2006; Zehe & Blöschl, 2004). The second reason  
284 is the motivation to use remote sensing data in similar follow up studies, which are not yet accurate  
285 enough for modelling purposes but allow a general classification of the wetness status. Because (i)  
286 corresponding information on soil matric potential cannot be deduced at larger scale from remote  
287 sensing data and (ii) hysteresis in the soil water retention curve may lead to ambiguous thresholds, we  
288 focus here on soil water content measurements.

289 Another choice for the model framework that must be discussed is the choice of percentile thresholds.  
290 From a soil hydrological point of view, it would make sense that the thresholds defining the three classes  
291 'wet', 'moderate' and 'dry' are chosen individually for each lysimeter (a wet clay soil may have very  
292 different water content values than a sandy soil). However, from a methodological point of view, we  
293 prefer to ensure that the model does not require a long time series to determine quantiles of soil water  
294 content data and that the model can be run solely based on the training site's distribution. Accordingly,  
295 the same percentile thresholds, derived from the training site, were applied to label daily water content  
296 values at the prediction sites. Note, that the application of the same percentile thresholds for all sites is

297 not relevant for the detection of changes in the soil water content response function. Very similar results  
298 will be obtained for a site-specific percentile definition as shown in the supplementary material (section  
299 S1). After constructing all the above features, each daily input to the model consisted of (i) raw climate  
300 variables (P, PET, and WB), (ii) the STL-derived seasonal and trend components for each of those  
301 variables (six variables), and (iii) the categorical moisture label. All ten features were aligned by date  
302 to ensure consistency across inputs. This combination of raw values, decomposed temporal signals, and  
303 qualitative soil condition provides the model with a detailed daily representation of both external  
304 climatic forcing and internal system state.

### 305 2.3 Neural Network Architecture and Training

306 To model daily volumetric soil water contents, a feed-forward neural network was implemented. The  
307 architecture consisted of three hidden layers: two dense layers with 12 neurons each using ReLU  
308 activation functions (Rectified Linear Unit), followed by a batch normalization layer, and a third dense  
309 layer with 6 neurons. ReLU was chosen for its ability to introduce non-linearity while maintaining  
310 computational efficiency and avoiding vanishing gradient problems during training (Lu et al., 2020;  
311 Montesinos López et al., 2022). Batch normalization was applied to stabilize learning by reducing  
312 internal covariate shift, which improves convergence speed and training stability (Montesinos López et  
313 al., 2022). The output layer consisted of a single neuron with a linear activation function, which is  
314 standard for continuous regression tasks such as predicting soil water content.

315 The network was trained using input features derived from daily observations at the reference lysimeter  
316 at the Bad Lauchstädt site, covering the period 2015–2023. Prior to training, all continuous input  
317 features were standardized to have a mean of zero and a standard deviation of one using z-score  
318 normalization. The standardization parameters (mean and standard deviation) were computed solely  
319 from the training dataset and applied unchanged to the validation and test sets at the training site, as  
320 well as to the prediction sites, ensuring consistency across all data splits. The target variable, volumetric  
321 soil water content, was preserved in its original physical units ( $\text{m}^3 \text{m}^{-3}$ ), allowing for direct interpretation  
322 of the model outputs and associated errors in hydrologically meaningful terms. The model was compiled  
323 with the Adam optimizer, which adaptively adjusts learning rates and is widely used for its

324 computational efficiency and stable convergence (Kingma and Ba, 2015). Mean squared error (MSE)  
325 was used as the loss function due to its sensitivity to large deviations, making it suitable for continuous  
326 regression tasks. To monitor generalization, 30% of the data was withheld as a validation set and  
327 excluded from updating the weights between the nodes during training. The training procedure was  
328 initially set to proceed for a maximum of 1000 epochs. To prevent overfitting, an early stopping  
329 criterion was implemented based on validation loss. Specifically, training was terminated if no  
330 improvement in validation performance was observed over a predefined number of consecutive epochs  
331 (patience threshold). The model parameters from the epoch exhibiting the lowest validation loss were  
332 retained for final evaluation.

## 333 2.4 Testing the Neural Network

334 After training, the model was applied to the remaining 23 lysimeters across both Selhausen and Bad  
335 Lauchstädt, none of which were included in the training phase. All test inputs were processed using the  
336 same structure and normalization parameters derived from the training data. As outlined in Section 2.1,  
337 the experimental setup includes four soil types, each installed with three replicates at both sites (see Fig.  
338 3). While the lysimeters at the Bad Lauchstädt lysimeter station share the same climatic setting as the  
339 training site, the lysimeters at Selhausen represent a more humid region. Accordingly, the raw data and  
340 seasonal trend data of the Selhausen climate were used as input for the prediction of soil water content  
341 in lysimeters located at Selhausen. This configuration allows to evaluate (i) whether the soil water  
342 content response function determined for the training remains valid for different climates and soil types,  
343 and (ii) to detect potential temporal changes in soil hydraulic behaviour. The evaluation and  
344 classification procedures are described in the following two subsections.

## 345 2.5 Detection of Change in Soil water content Response Function Based on Error 346 Metrics

347 As explained in the introduction, we use error metrics to detect changes in the soil water content  
348 response function. While we use the Nash-Sutcliffe efficiency (NSE, see eq. 5) as a general descriptor  
349 of model error, we investigate temporal changes in model performance based on the Mean Bias (MB)  
350 that was calculated on an annual basis from 2015 to 2023. This year-by-year assessment does not rely

351 on predefined change points and enables the detection of gradual or abrupt shifts in model performance  
352 directly from the data. MB measures the average signed difference between predicted and observed  
353 values, providing an estimate of systematic overestimation or underestimation over time (Moriassi et al.,  
354 2007; Liu et al., 2011) and is defined as:

$$355 \quad MB = \frac{1}{N} \sum_{i=1}^N (\hat{\theta}_i - \theta_i) \quad (1)$$

356 where  $\hat{\theta}_i$  is the predicted volumetric water content at day  $i$ ,  $\theta_i$  is the corresponding observation and  $N$   
357 defines the number of available observations–prediction pairs. Although, the calculation uses daily  
358 values, MB is aggregated over yearly intervals to produce a single value per year, capturing annual  
359 patterns in prediction bias. Volumetric water contents ( $\text{m}^3 \text{ m}^{-3}$ ) were multiplied by 100 prior to  
360 calculation, and MB is therefore reported in percentage (%). Positive MB values indicate systematic  
361 overestimation by the model, while negative values reflect underestimation. The annual assessment of  
362 MB allowed us to evaluate whether the soil water content response function remains consistent over  
363 time or shows temporal dynamics. Deviations between predicted and observed water content can differ  
364 in sign across moisture conditions and event types, such that opposite errors may partially cancel when  
365 averaged over a full year. Therefore, mean bias is interpreted as an indicator of long-term temporal drift  
366 in model–observation differences, while soil water retention curves are used here (see next section) to  
367 verify the physical consistency and direction of detected changes; in cases where retention  
368 measurements are not available, robustness of bias trends can alternatively be assessed by repeating the  
369 analysis using different temporal aggregation periods.

370 To classify the soil water content dynamics with respect to the resilience after the extreme summer  
371 2018, we check if the deviation of the predictions based on a stable response function (developed with  
372 the training data) changes over the years. When the deviation in the first year (2015; i.e., before the  
373 drought) is different from the deviation in the year 2023, we consider that the soil water content response  
374 function has changed (it is still possible that the response function may recover in the future) and the  
375 soil water content dynamics is classified accordingly as ‘changed’. When the deviations at beginning  
376 and end are similar, but there was a period between 2018 and 2022 with a different deviation level, we  
377 conclude that the soil water content response function changed reversibly over time but recovered

378 within the observation window and the lysimeter is classified as ‘resilient’. Note that in resilience-  
 379 related literature, the system response to disturbance is often characterized by the time scale and rate of  
 380 recovery following perturbation (Scheffer et al., 2009). Here, we do not analyse the recovery rate in  
 381 more detail but based on the definition of the ‘resilient’ category the recovery rate must be smaller than  
 382 four years.

383 The soil water content response is considered as ‘stable’ when the deviations remain similar during the  
 384 entire observation period (i.e., the same response function of soil moisture dynamics to climatic  
 385 condition can be used). As threshold we chose 1.52%, that equals the 3-fold of the standard deviation  
 386 of the nine yearly MB values computed for the training site. The classification of the time series was  
 387 thus expressed formally as:

388 ‘changed’:  $|MB_{2023} - MB_{2015}| > 1.52\%$  (2)

389 ‘resilient’:  $|MB_{2023} - MB_{2015}| \leq 1.52\% \wedge |MB_{20xx} - MB_{2015}| > 1.52\%$  (3)

390 ‘stable’:  $|MB_{2023} - MB_{2015}| \leq 1.52\% \wedge |MB_{20xx} - MB_{2015}| \leq 1.52\%$  (4)

391 with the logical operator  $\wedge$  and the mean bias of a specific year with  $MB_{20xx}$ , that shows the largest  
 392 difference  $|MB_{\text{year}} - MB_{2015}|$  for the time period between 2018 and 2022 (starting with dry year 2018).

393 As general information on the different response function, we calculated the Nash–Sutcliffe efficiency  
 394 (NSE) coefficient (Moriassi et al., 2007; Nash & Sutcliffe, 1970). The NSE is a standard metric for  
 395 hydrological model skill, with  $NSE = 1$  indicating perfect agreement and  $NSE \leq 0$  stating that the model  
 396 predictions are no better than using the mean of the observations. Mathematically, it is defined as:

397 
$$NSE = 1 - \frac{\sum_{i=1}^N (\theta_i - \hat{\theta}_i)^2}{\sum_{i=1}^N (\theta_i - \bar{\theta})^2} \quad (5)$$

398 where  $\hat{\theta}_i$  is the predicted volumetric water content at day  $i$ ,  $\theta_i$  is the corresponding observed value,  $\bar{\theta}$  is  
 399 the mean observed volumetric water content over the evaluation period, and  $N$  denotes the total number  
 400 of valid data points used in the calculation. Following Moriassi et al. (2015), model performance was

401 classified as very good for  $NSE > 0.80$ , good for  $0.70 < NSE \leq 0.80$ , satisfactory for  $0.50 < NSE \leq 0.70$ ,  
402 and unsatisfactory for  $NSE \leq 0.50$ .

403 In this study, NSE is used to summarize the overall agreement between simulated and observed soil  
404 water dynamics, whereas the identification and classification of temporal changes in the soil water  
405 content response function rely exclusively on the annual evolution of mean bias. Lower NSE values  
406 were interpreted as reduced dynamic agreement between the tested lysimeter and the reference soil–  
407 climate response used for training, without implying a specific mechanism of change.

## 408 2.6 Interpretation of Change in Response Function in Soil Physical Terms

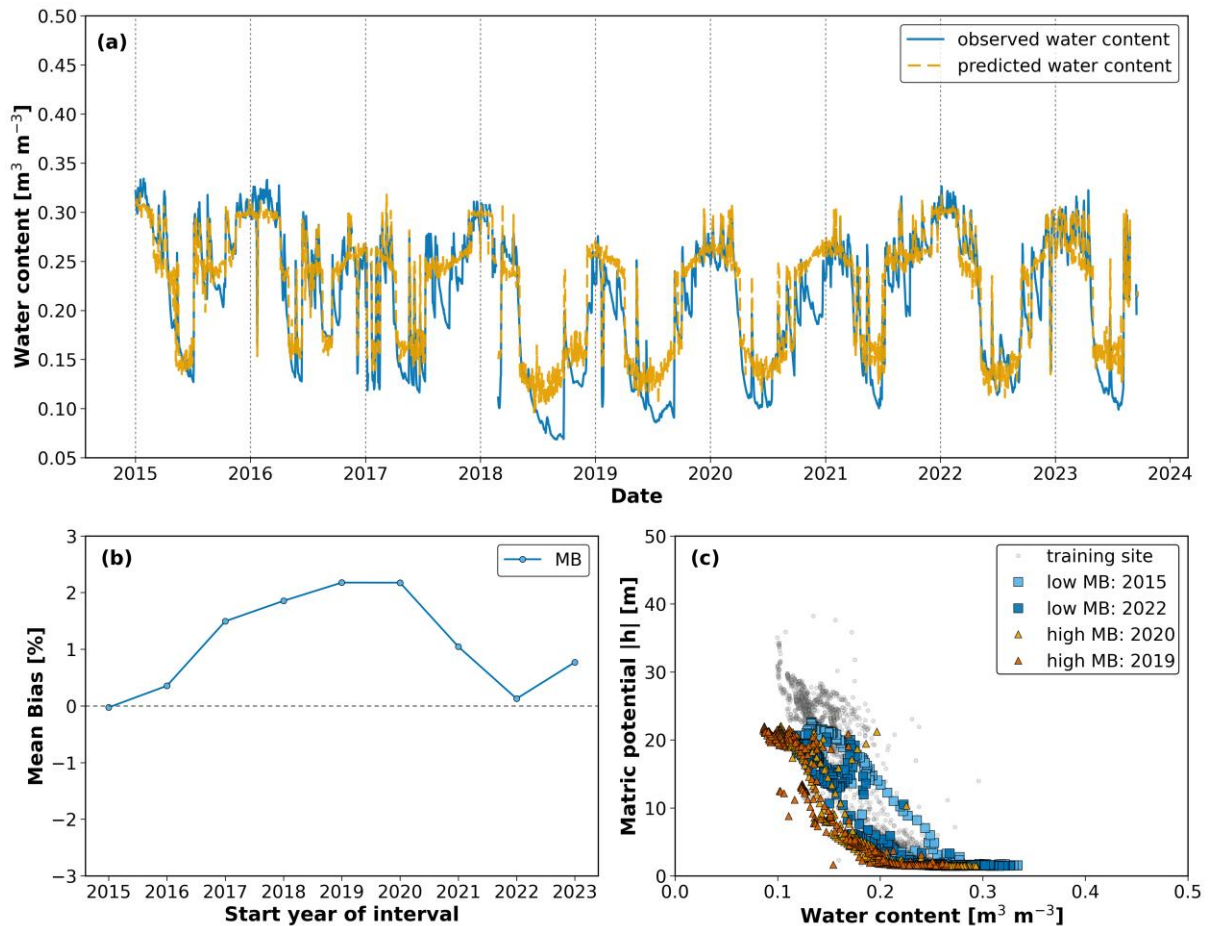
409 The dynamics of MB (see above) was also used to assess changes in soil water retention curves  
410 (SWRCs), which were plotted for each test lysimeter on a yearly basis. As stated in eq. (1), a positive  
411 MB value corresponds to measured water contents values that are smaller than the predictions. Because  
412 the predictions are based on the model trained for a specific lysimeter, we expect for a positive MB that  
413 the water content for the same environmental conditions (as manifested in the matric potential) is  
414 smaller in the test lysimeter compared to the lysimeter used for training (SWRC is shifted to the left).  
415 Analogously, for a consistently negative MB we expect that the test site retained more water at a given  
416 matric potential than the training site and the SWRC is shifted to the right. For a ‘resilient’ soil, the soil  
417 water retention curve will be shifted over time and will shift back close to the original position at the  
418 end of the observation period. Finally, for a soil with ‘changed’ response function, the water retention  
419 curve is drifting over time as well but without returning to its original position. In some cases, the  
420 temporal evolution of MB may not exactly follow the apparent shift of the SWRC, as additional vertical  
421 or slope changes could occur due to variations in porosity or pore-size distribution. These effects cannot  
422 be identified within the current framework but may contribute to deviations between MB dynamics and  
423 the apparent SWRC shift. To further support the SWRC-based interpretation, a quantitative analysis of  
424 soil water retention curve evolution based on the concept of integral mean water content is provided in  
425 the Supplementary Material.

## 426 3. Results

427 Following the methodological framework described in Section 2.3-2.6, we present the results of model  
428 predictions across the test lysimeters to assess the resilience of the soil water content response function  
429 for the different lysimeters. We organize the section in four subsections according to the four different  
430 origins of the soil in the lysimeters (see Fig.3b) to discuss effects of soil origin and climatic conditions  
431 on the response function. In the last subsection (3.5) the results are summarized to allow direct  
432 comparison of all 24 lysimeters. Note, that all model results presented below are based on the soil water  
433 content classification ('wet', 'moderate', 'dry') as deduced from the lysimeter used for model training.  
434 The corresponding figures using specific classification for each lysimeter are shown in supplementary  
435 information Fig. S4-S7.

### 436 3.1 Lysimeters with same soil as used in model training (Dedelow soils)

437 The neural network was trained to capture the soil water content response function of one lysimeter  
438 with sandy loam topsoil (Luvisol) extracted from Dedelow and translocated to the dry climatic region  
439 in Bad Lauchstädt (see Fig. S1 in supplementary material). The NSE of the training and validation of  
440 that specific lysimeter was very high with 0.91 indicating good model performance. The application of  
441 this response function to the other two lysimeters from Dedelow that were translocated to Bad  
442 Lauchstädt in relatively high NSE (0.79 and 0.84), but the response in summer 2018 with lower soil  
443 water content was not captured properly as shown in Fig. 5a. More specifically, the time series show  
444 that predictions and observations matched closely in 2015, while after the dry summer of 2018 the  
445 model systematically overestimated water content in 2019 and 2020, before the agreement improved  
446 again towards the end of the period.



447  
 448 **Figure 5** Analysis of soil water content dynamics (2015–2023) for a Dedelow-origin lysimeter tested at Bad  
 449 Lauchstädt. Panel (a) shows the time series of observed (blue) and predicted (orange) water content, with close  
 450 agreement in 2015, clear overestimation in 2019–2020 (predictions above observations), and improved  
 451 agreement again towards the end of the period. Panel (b) presents the temporal evolution of mean bias (MB),  
 452 remaining near zero until 2017, increasing to about 2–3 % in 2019–2020, and decreasing again to approximately  
 453 zero in 2022. Such soil water content response was classified as ‘resilient’. Panel (c) displays soil water retention  
 454 curves from the training site (grey) and from selected years representing different MB conditions, with low-MB  
 455 years (2015, 2022) and high-MB years (2019, 2020). The curves are close to the training site in 2015, show a  
 456 shift to lower water contents in 2019–2020, and in 2022 return to the training site data.

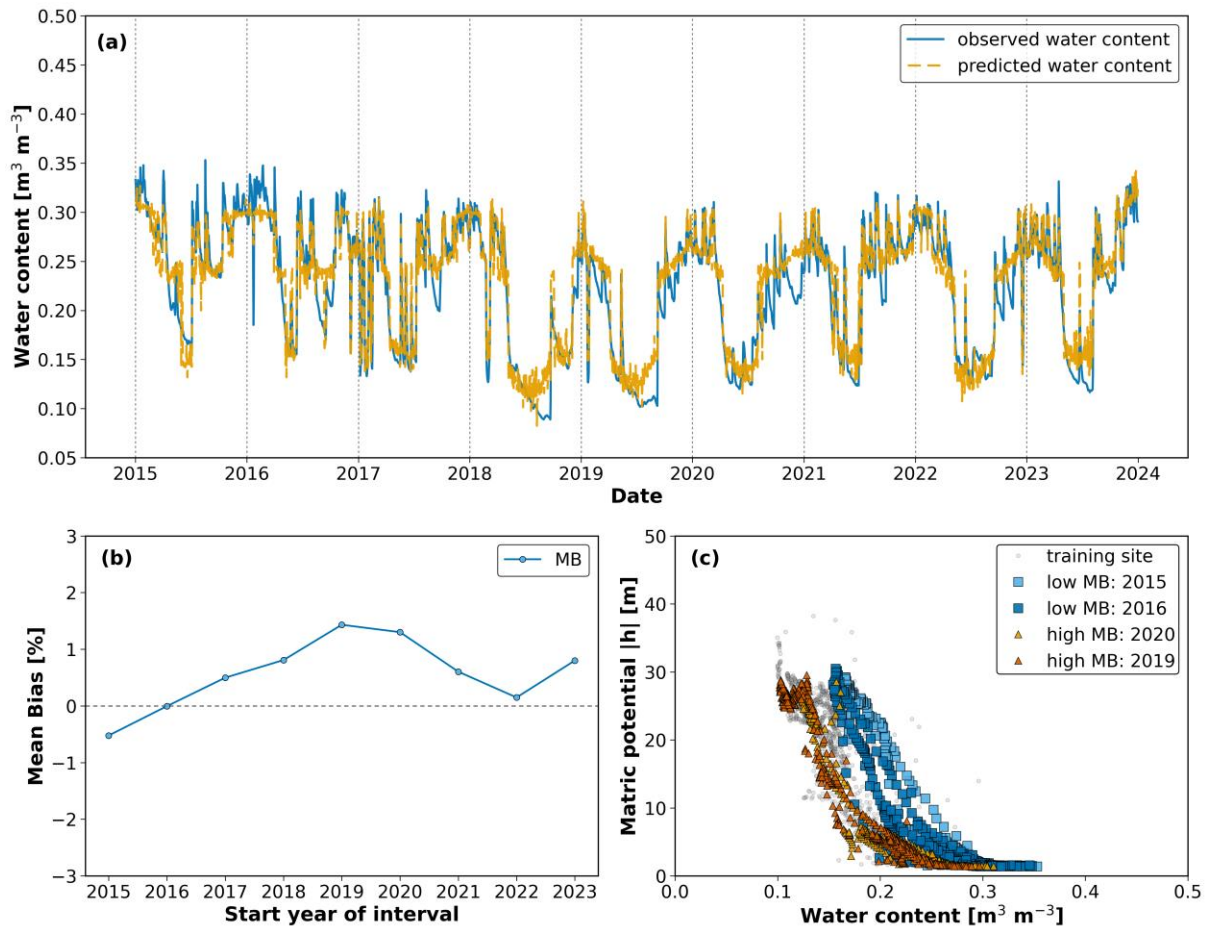
457 These changes are reflected in the MB development (Fig. 5b), with values increasing from near zero in  
 458 2015 to about 2–3% in 2019–2020 and then decreasing again towards 2022. The retention curves  
 459 confirm this interpretation (Fig. 5c). The year with low MB (2015) produced a SWRC close to the  
 460 measured curve of the training site, the years with high MB (2019–2020) were shifted to lower water  
 461 contents, and the later year with reduced MB (2022) returned to the measured SWRC of the training  
 462 site. Taken together, the time series, MB trend, and SWRCs show that the soil response was disturbed  
 463 after 2018 but later recovered, defining this lysimeter as ‘resilient’. The same finding holds for the

464 simulations for the lysimeters translocated to Selhausen (less dry climate) with high NSE between 0.80–  
465 0.82. This indicates that for the coarse-textured soil included in this study (i) the effect of changing  
466 climatic conditions was rather small (very good NSE classification for both sites), but (ii) that these  
467 coarse-textured topsoils do not show identical response to the extreme year, as each lysimeter reacts  
468 slightly differently, which may indicate small differences in hydraulic properties.

### 469 3.2 Lysimeters with soils formed under the same climate as the one used in model 470 training (Bad Lauchstädt soil)

471 The lysimeters filled with soil from Bad Lauchstädt (Chernozem) were formed under the climatic  
472 conditions used for the fitting of the response function. In case of dominant effect of climate on the soil  
473 water content response function, we could expect similar results as for the training lysimeter. For the  
474 soil remaining at the original site (Bad Lauchstädt), the model performance was very good (0.88–0.89).  
475 As shown for an example in Fig. 6a, the fit between observed and predicted water content was  
476 consistently close, with a tendency to slightly underestimate in the early years and to mildly  
477 overestimate after 2018, particularly in 2019–2020, before the agreement improved again in later years.  
478 This is also manifested in the MB values that increased from slightly negative values in 2015 to about  
479 +1.5% in 2019, before decreasing again towards zero (Fig. 6b). The plotted SWRCs support this  
480 interpretation (Fig. 6c), with low MB years (2015 and 2016) showing a slight shift to higher water  
481 contents relative to the measured SWRC of the training site, and high-MB years (2019 and 2020)  
482 displaying a modest shift to lower water contents. Accordingly, the soil water content dynamics was  
483 classified as ‘resilient’.

484 For the lysimeters transported from Bad Lauchstädt to Selhausen, the performance was more variable  
485 (NSE ranging from 0.50 to 0.84) corresponding to satisfactory to very good classifications, reflecting  
486 the stronger effect of the wetter climate. None of the three lysimeters that stayed in Bad Lauchstädt  
487 were classified as ‘changed’ but two out of three showed a systematic shift and were classified as  
488 ‘changed’ when translocated to Selhausen (see Table 1). In short, these examples show that the Bad  
489 Lauchstädt soil remained resilient under its original climatic conditions at Bad Lauchstädt but changed  
490 when exposed to the wetter climatic conditions at Selhausen.

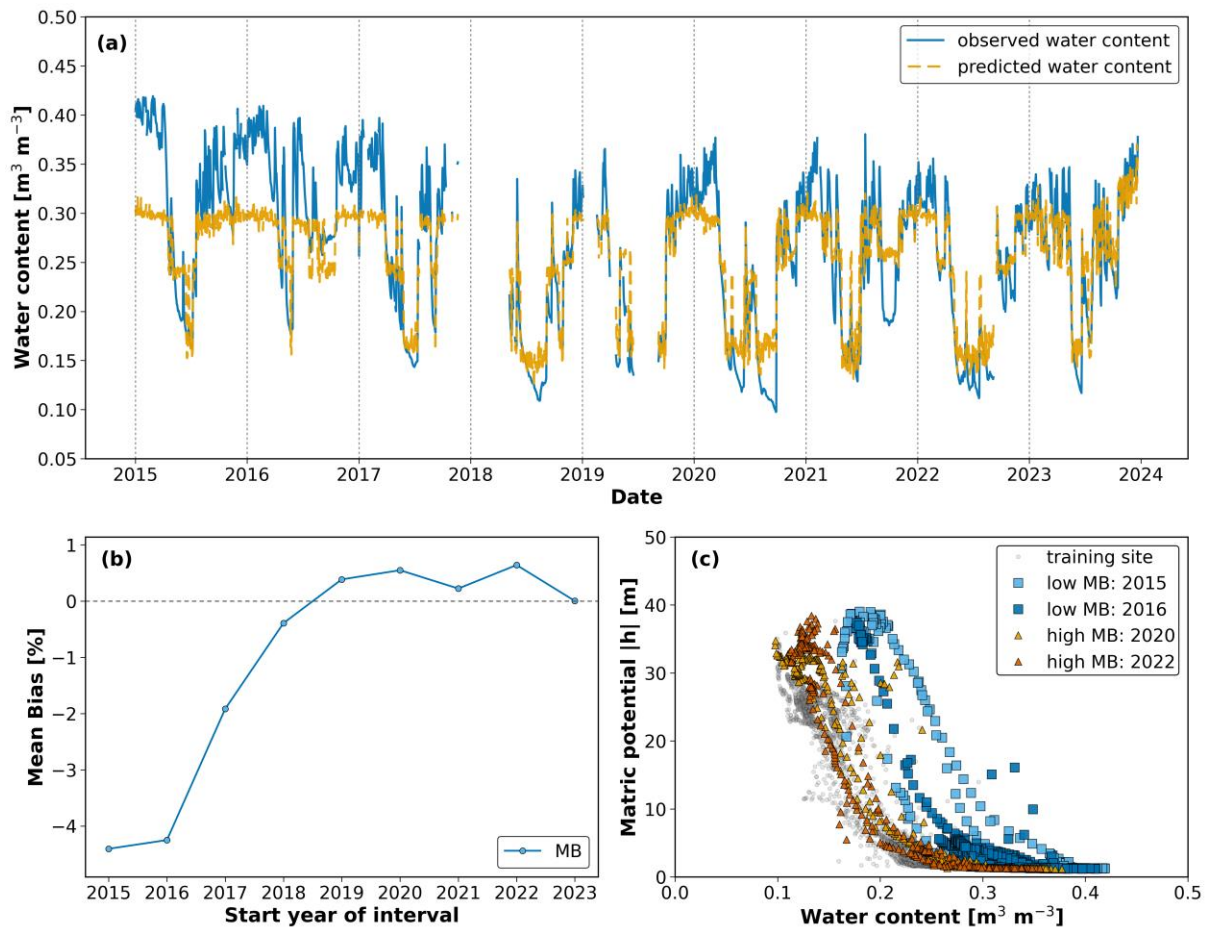


491 **Figure 6** Analysis of soil water content dynamics (2015–2023) for a Bad Lauchstädt-origin soil lysimeter tested  
 492 at Bad Lauchstädt. (a) Comparison of measured (blue) and simulated (orange) daily water content values,  
 493 showing high agreement in the early years and temporary overestimation in 2019–2020. (b) Mean Bias (MB)  
 494 started slightly negative in 2015, increased to about +1.5 % in 2019, and then decreased again towards 2022. (c)  
 495 Soil water retention curves (SWRCs) from the training site (grey) and from the same replicate for selected years  
 496 with low MB (2015, 2016) and high MB (2019, 2020) show close agreement in the early years and a shift to lower  
 497 water contents in 2019–2020.  
 498

### 499 3.3 Lysimeters with soils formed under similar climate as the one used in model 500 training (Sauerbach soil)

501 The findings are similar for the silt loam (Cambisol) from Sauerbach that was formed under similar  
 502 climatic condition as those in Bad Lauchstädt. As in case of the soil from Bad Lauchstädt, soils from  
 503 Sauerbach show higher NSE values when translocated to Bad Lauchstädt (0.81–0.88, very good)  
 504 compared to those transferred to the wetter climate in Selhausen (0.74–0.79, good). This reflects, that  
 505 the soil water content response function in the drier climate is not the same as in the wetter climate. In  
 506 one illustrative case, the observed water content initially showed wetter dynamics than predicted, but

507 gradually converged toward the model predictions by 2023, indicating a possible adjustment in soil  
 508 hydraulic response over time (Fig. 7a).



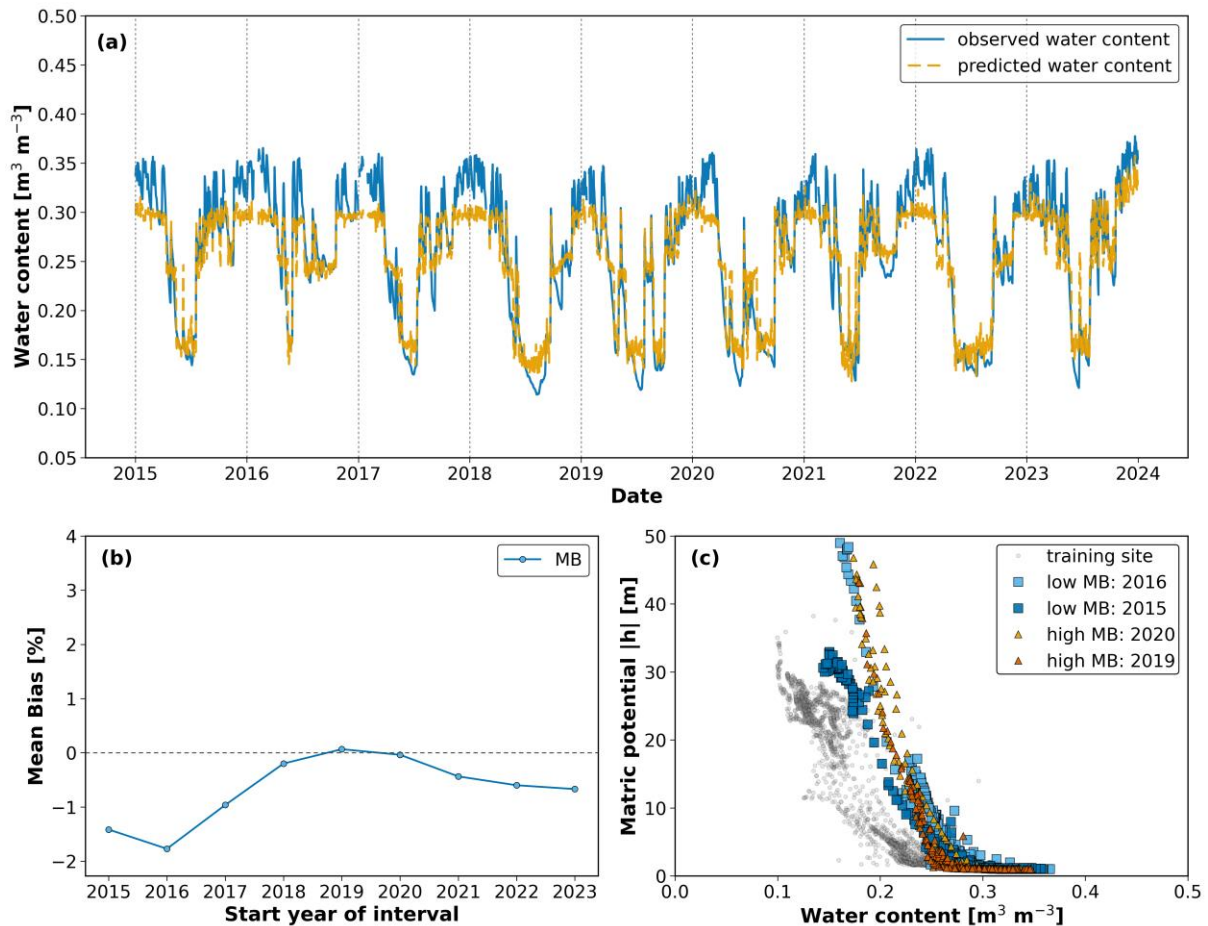
509 **Figure 7** Analysis of soil water content dynamics (2015–2023) for Sauerbach-origin lysimeter relocated to  
 510 Selhausen (a) Comparison of observed and predicted daily volumetric water content ( $NSE = 0.74$ ) After initial  
 511 underestimation by the model, the observed and predicted values gradually converged, indicating a possible  
 512 adjustment in soil hydraulic behaviour over time. (b) Temporal evolution of the mean bias (MB), which increased  
 513 from about  $-5\%$  in 2015 to values close to zero by 2019–2023, consistent with the improved match between  
 514 observed and predicted values shown in panel (a). (c) Soil water retention curves (SWRCs) from the training site  
 515 (grey) and from selected years with low MB (2015, 2016) and high MB (2020, 2022) illustrate the same trend,  
 516 with early years showing higher water contents at a given matric potential and later years shifting towards to the  
 517 training curve.  
 518

519 This development is also evident in the MB values (Fig. 7b), which started strongly negative ( $-5\%$ ) in  
 520 2015–2016 and steadily increased toward values close to zero by 2023, indicating a progressive  
 521 reduction of underestimation. The corresponding SWRCs (Fig. 7c) confirm this trend, with curves from  
 522 early years (2015, 2016) showing higher water contents at a given matric potential compared to the  
 523 measured SWRC of the training site and later years (2021, 2023) shifting closer to the reference,

524 suggesting a gradual adjustment of hydraulic behaviour. In the case of soils from Sauerbach, there was  
525 a difference in quantification of resilience with respect to the classification of the soil water content  
526 used as input variable: with the classification based on the training lysimeter (with sandy loam in the  
527 topsoil), the soil water content dynamics was classified as ‘changed’ for all six lysimeters. But using  
528 the classification based on the soil water content statistics obtained for each lysimeter individually (see  
529 Fig. S6), the large water contents at the beginning were captured and only one lysimeter out of three  
530 was classified ‘changed’. Independent of the water content classification, all lysimeters translocated to  
531 Selhausen were classified as ‘changed’, exhibiting the strongest response to relocation of all soils.

### 532 3.4 Lysimeters with soils formed under different climate compared to the one used 533 in model training (Selhausen)

534 At last, we discuss the Selhausen silt loam (Luvisol), which was formed under weather conditions that  
535 were not used in the training of the neural network. The model performance was better for the replicates  
536 translocated to the drier Bad Lauchstädt climate (NSE = 0.86–0.92, very good), compared to slightly  
537 lower performance at their site of origin under humid Atlantic conditions (0.76–0.86, good to very  
538 good). The classification with respect to resilience helps to explain this, since Selhausen soils at their  
539 origin were mainly assigned to ‘stable’ or ‘resilient’ categories (see Table I), while the same soils  
540 translocated to Bad Lauchstädt showed a more variable pattern. This indicates, that the lower NSE at  
541 Selhausen does not represent a misfit of the model but reflects that the soils follow their own stable soil  
542 water content response function. One replicate at Selhausen (NSE = 0.85) reproduced the seasonal  
543 dynamics well, although differences between observed and predicted values remained visible in the wet  
544 season across several years (Fig. 8a). The MB shifted from negative values in the first years toward  
545 zero after 2019. Note, that an MB value of 0 does not mean that deviations disappeared, but that errors  
546 in wetter and drier phases compensated each other (Fig. 8b). The SWRCs were generally close to the  
547 training reference, but in later years small deviations appeared mainly at the saturated end (Fig. 8c).  
548 Overall, these changes remained below the assumed threshold, supporting a classification of the soil  
549 water content dynamics as ‘stable’.

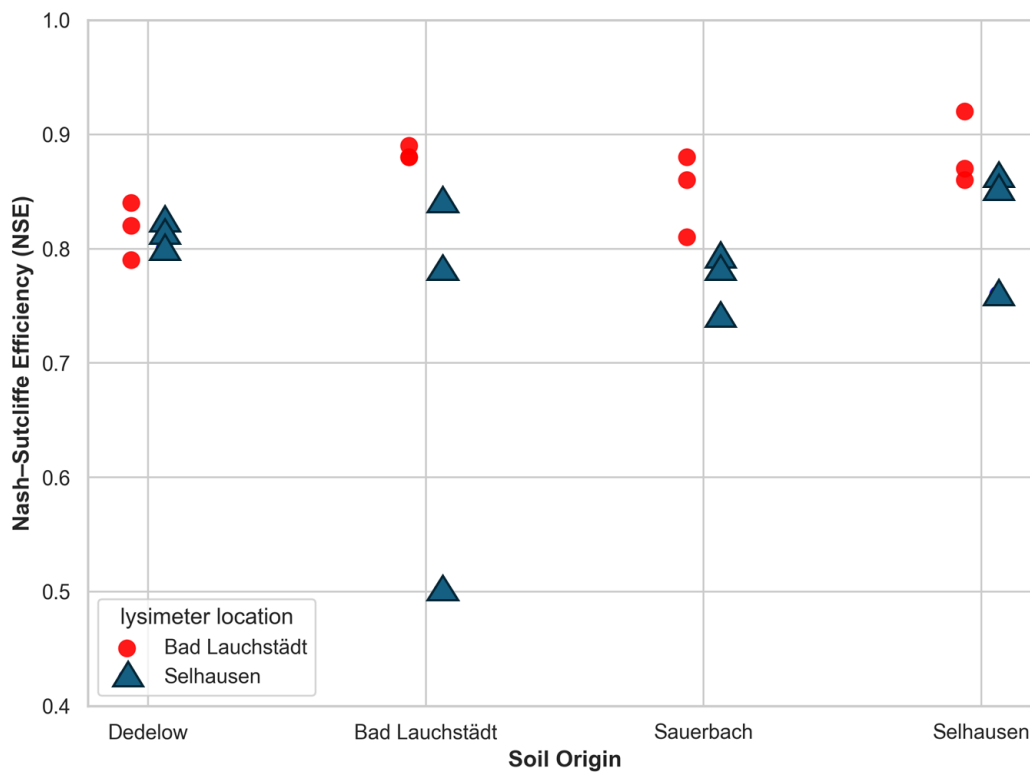


550 **Figure 8** Soil water content dynamics (2015–2023) for a Selhausen-origin lysimeter tested at Selhausen. (a)  
 551 Observed (blue) and predicted (orange) water content show fair agreement, with underestimation of water  
 552 contents in the wet season. (b) Mean Bias (MB) fluctuated from negative values in the early years to values close  
 553 to zero after 2019, but these variations remained below the threshold for change. (c) Soil water retention curves  
 554 (SWRCs) from the training site (grey) and from selected years with low MB (2015, 2016) and higher MB (2019,  
 555 2020) reflect these minor variations, with the 2019 curve showing the strongest deviation yet remaining close to  
 556 the training reference, consistent with the stable classification. The apparent cutoff at the wet end in (a) arises  
 557 from the use of absolute rather than normalized values during training, as discussed in the Supplementary  
 558 Material (Text S1).  
 559

### 560 3.5 Comparison of all lysimeters

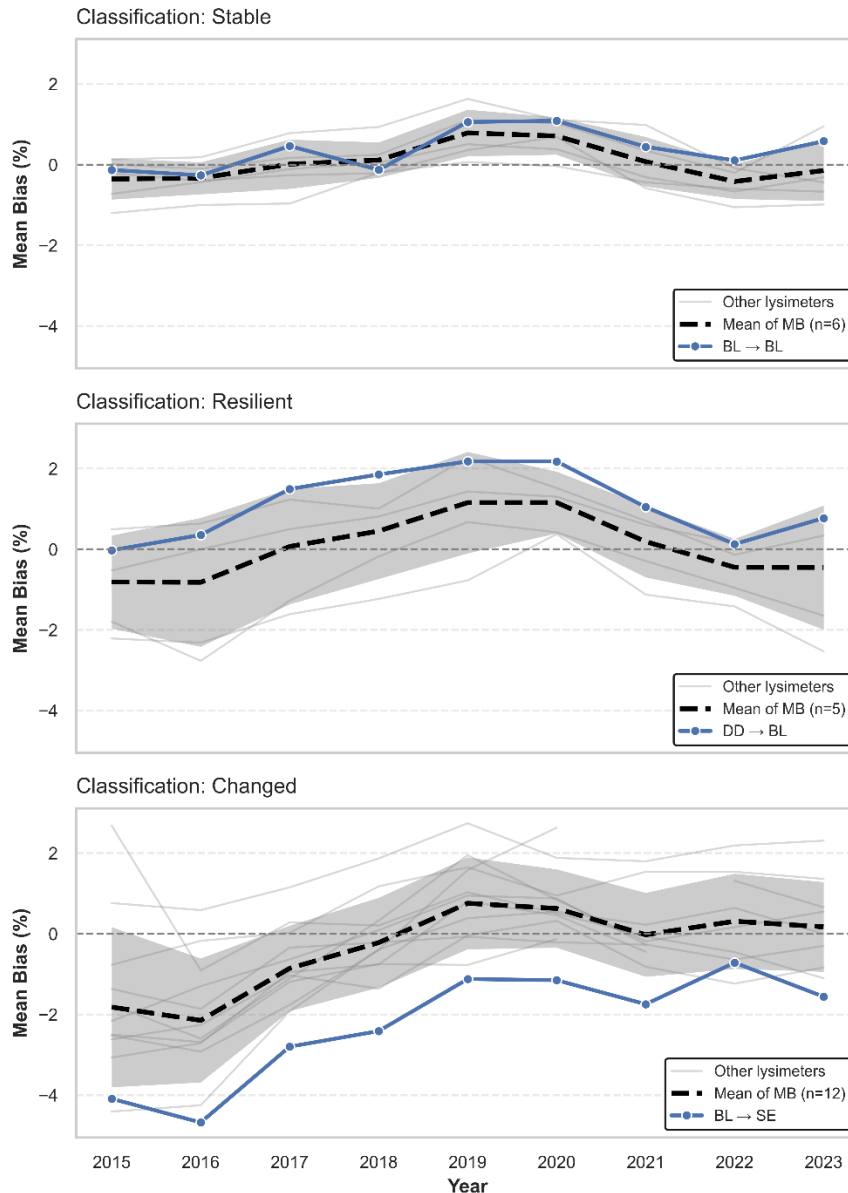
561 The comparison of the soil water content dynamics of all lysimeters indicate, that contrasting climatic  
 562 conditions between sites—particularly between the continental Bad Lauchstädt and Atlantic-influenced  
 563 Selhausen—can significantly alter the hydraulic response of the soil, even when texture remains  
 564 constant. In general, prediction performance at Selhausen was lower, likely because the model was  
 565 trained under the drier climate of Bad Lauchstädt, and therefore, failed to fully capture the soil–water

566 interactions emerging under wetter conditions (Fig. 9). The broader NSE range observed at Selhausen  
 567 location further suggests increased variability in hydraulic response among replicates.



568 **Figure 9** Spread of Nash–Sutcliffe efficiency (NSE) values across different soil origins and test locations. Each  
 569 symbol represents one lysimeter from a given origin (x-axis) evaluated at Bad Lauchstädt or Selhausen (indicated  
 570 by colour). The results highlight the influence of climate–soil interactions on model performance. Notably, Bad  
 571 Lauchstädt-origin soils exhibited strong performance at their origin but a wider and lower range when tested at  
 572 Selhausen, indicating increased variability in soil hydraulic behaviour and divergence in soil–climate response.  
 573

574 With respect to resilience of the soil water content response function, we show the temporal evolution  
 575 of the mean bias for all lysimeters in Fig. 10 and summarize the results in Table 1. In Table 1 we add  
 576 the general classification type (‘stable’, ‘resilient’ and ‘changed’) and calculate the average of 3  
 577 lysimeters (same material and same location) for the drift in mean bias value between the year 2015  
 578 and 2023 and the maximum deviation from year 2015 for the years between 2018 and 2022. The table  
 579 shows that deviations from a ‘stable’ or ‘resilient’ response function mainly occur when soils from  
 580 Dedelow, Bad Lauchstädt, and Sauerbach were translocated to Selhausen. Only in case of the soil from  
 581 Selhausen, the response function remains ‘stable’. It seems, that the soil material ‘trained over decades’  
 582 to the wetter climate in Selhausen adapts better to the extreme summer 2018.



583  
 584 **Figure 10** Temporal evolution of Mean Bias (MB) for three representative lysimeter replicates, each classified  
 585 into one of three soil hydraulic response categories: (a) 'stable', (b) 'resilient', and (c) 'changed'. Thick dashed  
 586 lines indicate the mean of the MB trend across all lysimeters within each classification group, with sample size  
 587 ( $n$ ) specified in the legend. Shaded areas represent  $\pm 1$  standard deviation. Thin grey lines show individual MB  
 588 trajectories of the remaining lysimeters in each group. Highlighted blue lines depict selected replicates  
 589 originating from and/or tested at distinct sites: (a) BL  $\rightarrow$  BL (soil material from Bad Lauchstädt tested at its  
 590 origin), (b) DD  $\rightarrow$  BL (soil material from Dedelow tested at Bad Lauchstädt), and (c) BL  $\rightarrow$  SE (soil material  
 591 from Bad Lauchstädt tested at Selhausen). These examples illustrate contrasting temporal patterns in hydraulic  
 592 response, ranging from sustained stability to progressive divergence from the trained site dynamics.

593 **Table 1:** Resilience of soil water content response function for the four soil materials translocated to Bad  
 594 Lauchstädt and Selhausen. The 'type' describes the class of response function of the individual lysimeters (S for  
 595 'stable', R for 'resilient' and C for 'changed'). The 'drift' is the average value  $|\text{MB}_{2023} - \text{MB}_{2015}|$  of the three  
 596 lysimeters with the difference in Mean Bias (MB) between years 2023 and 2015. The 'amplitude' is the maximum

597 difference of the Mean Bias between the first year (2015) and the years between 2018 and 2022 (denoted as year  
 598 20xx).

	Located at Bad Lauchstädt			Located at Selhausen		
	Type	Drift	Amplitude	Type	Drift	Amplitude
Dedelow	<b>S, R, C</b>	1.09	1.76	<b>R, C, C</b>	1.72	2.11
Bad Lauchstädt	<b>S, S, R</b>	0.94	1.36	<b>R, C, C</b>	2.15	2.99
Sauerbach	<b>C, C, C</b>	2.17	3.73	<b>C, C, C</b>	3.38	4.24
Selhausen	<b>S, R, C</b>	0.96	2.24	<b>S, S, R</b>	0.47	1.78

599

## 600 4. Discussion

601 The results presented in Section 3 demonstrate that the model can reproduce soil water content dynamics  
 602 reliably under stable conditions (as indicated by high NSE-values), but it exhibits limitations when soils  
 603 undergo persistent changes in hydraulic behaviour or are exposed to a different climate. Several soils  
 604 showed a shift in the wet range, indicating that differences in soil water content response cannot be  
 605 explained by texture alone but reflect the combined effects of climatic conditions and structural  
 606 evolution. Based on these findings, the following discussion evaluates how assumptions of static  
 607 hydraulic behaviour and response function affect model performance, examines the role of NSE and  
 608 MB in identifying evolving system dynamics, and reflects on the broader implications for long-term  
 609 modelling and soil water content monitoring.

### 610 4.1 Soil–Climate Interactions as Drivers of Hydraulic Response Function

611 The predictive success of data-driven models depends not only on the physical properties of soils but  
 612 also on the climatic context in which those properties developed and continue to function. The present  
 613 study shows that soils exhibit the most consistent replicate behaviour when evaluated under climate  
 614 conditions similar to those of their origin, where gradual climatic changes over time have allowed their  
 615 structure to adjust naturally. When exposed to faster or contrasting climatic shifts, as in translocated  
 616 settings, the soil response becomes less predictable and less stable. This can be shown using the table  
 617 S1 in the supplementary material file, which lists the average trends (difference in MB between year  
 618 2023 and 2015) and amplitudes (difference in MB between 2015 and the dry years) for three lysimeter  
 619 replicates: only for the three lysimeters at the original locations Bad Lauchstädt or Selhausen), both

620 drift and amplitude were below the stability threshold of 1.52% and can classified as ‘stable’ as group  
621 of lysimeters.

622 This suggests that the function of the soil system cannot be meaningfully decoupled from its climatic  
623 history. Soils may develop pore arrangements, aggregation patterns, and, as a consequence, moisture  
624 retention characteristics that reflect long-term adaptation to local hydrological regimes. When these  
625 soils are translocated to environments with contrasting precipitation and atmospheric demand, their  
626 hydraulic response can shift in ways that are not captured by static texture-based estimates of soil  
627 hydraulic properties. Alternative pore-scale processes, including slowly reversible swell–shrink  
628 behaviour and non-equilibrium preferential flow, may also contribute to the observed shifts in apparent  
629 SWRC behaviour. Recent large-scale analyses have demonstrated statistically significant impacts of  
630 climatic factors on soil pore space organisation and laboratory-measured retention characteristics  
631 (Hirmas et al., 2018; Klöffel et al., 2024), providing independent support for the plausibility of climate-  
632 driven modification of soil hydraulic response.

633 Such context-dependent behaviour highlights the limitation of the common assumption that soils with  
634 the same texture will show comparable retention across regions, an assumption often made in the  
635 absence of better descriptors. While laboratory-measured SWRCs show strong and well-established  
636 correlations with texture across climatic gradients, particularly in the dry range, experimental evidence  
637 collected under natural field conditions indicates that this simplified description does not always hold  
638 (Hannes et al., 2016; Robinson et al., 2016; Aqel et al., 2024). In our case, even soils with similar  
639 textural composition exhibited different levels of model agreement depending on climate, highlighting  
640 that physical similarity (e.g. soil texture) does not guarantee functional equivalence in retention. For  
641 example, Selhausen-origin soils achieved higher NSE values when translocated to Bad Lauchstädt,  
642 likely because the model was trained under similar dry climatic conditions. However, classification  
643 results showed, that these soils retained greater stability at their origin, suggesting that predictive  
644 success under familiar climatic forcing does not necessarily imply hydraulic consistency. After the 2018  
645 drought, the Selhausen soils translocated to Bad Lauchstädt converged toward similar dynamics across  
646 replicates, with MB stabilizing close to zero, indicating that their response functions adjusted  
647 consistently to the drier climate (see Fig. S2 in the supplementary material). However, a clear carry-

648 over effect was observed: soil water in the upper 10 cm was not fully replenished during the wet phase  
649 of autumn and winter 2019 and only reached comparable, though slightly lower, values in winter 2020.  
650 A comparable multi-year legacy across the full soil column was reported in the TERENO-SOILCan  
651 lysimeter network by Groh et al. (2020).

652 All mentioned points underscore the importance of including very broad range of climatic forcing in  
653 the assessment of soil model transferability, as demonstrated by Groh et al. 2022. Our results also  
654 suggest that future efforts to generalize hydrological models should consider training under a range of  
655 climatic conditions to capture the full expression of soil–climate interactions, rather than relying on a  
656 single static representation. From a process-based perspective, these findings reflect that climate does  
657 not simply modulate soil water content inputs but actively shapes the retention and release behaviour  
658 of the soil pore network by driving changes in soil hydraulic response. While management practices  
659 across sites were similar, minor differences in tillage and fertilization cannot be completely excluded  
660 and may have influenced soil structure and water retention. In addition, monitoring of soil organic  
661 matter over time would be illustrative to link the change in the response function and structure related  
662 soil hydraulic properties to biological processes. Another mechanism that could result in structural  
663 changes is swelling and shrinking of the soils with considerable clay amount (three soils with ~20%  
664 clay). Nonetheless, the dominant control remains climatic forcing, which makes this consideration  
665 particularly relevant for climate-change experiments: models calibrated under past climatic conditions  
666 may not remain valid under the rapid climatic shifts projected for the coming decades. Neglecting this  
667 evolving soil–climate feedback could lead to substantial underestimation of future changes in soil  
668 hydraulic behaviour and associated ecosystem responses.

#### 669 4.2 High Predictive Performance Can Mask System Evolution

670 Although, several lysimeters achieved high predictive performance as expressed by high NSE values  
671 (Fig. 9), systematic trends in MB over time suggest that the underlying retention behaviour and soil  
672 water content response function may have shifted (Fig. 10 and Table 1). This was most apparent in  
673 Dedelow soils translocated to Bad Lauchstädt, where the model maintained high NSE values, but the  
674 MB increased across years (see Fig. S3). The corresponding shifts in the soil water retention curves

675 confirmed a gradual change in how the soil retained water, despite the model continuing to predict  
676 moisture levels accurately.

677 This suggests that local in hydraulic behaviour can occur without immediate deterioration in model fit.  
678 The predictive framework remained effective in capturing the general moisture dynamics, but the  
679 relationship between matric potential and water content was no longer consistent with that observed  
680 during training. These findings highlight that high model accuracy does not guarantee stability in the  
681 hydraulic characteristic, particularly under changing environmental conditions. Identifying such  
682 divergence early is critical for maintaining reliable predictions in long-term monitoring.

### 683 4.3 Implications for Monitoring, Remote Sensing, and Soil Health

684 The classification outcomes across all lysimeters highlight the role of site memory and hydraulic  
685 resilience in maintaining soil water response under climatic stress. Soils assessed at their origin were  
686 more frequently classified as ‘stable’ or ‘resilient’ (e.g., Selhausen at Selhausen), while those  
687 translocated to different locations were more likely to be classified as ‘changed’ (e.g., Sauerbach at Bad  
688 Lauchstädt). As was stated in the method section, this classification as ‘changed’ is affected by the  
689 length of the observation window and does not allow definitive decision between a persistent change to  
690 a new response function and a manifestation of a low recovery rate. Independent of future development,  
691 these patterns indicate that soil hydraulic behaviour shaped by long-term climatic adaptation may  
692 change when soils are exposed to new environmental conditions. The presented methods allow  
693 detection of emerging shifts in soil hydraulic behaviour that may be relevant for soil health assessment  
694 and could serve as indicators of deteriorating soil health status. The presented methods allow us to  
695 detect emerging hydrological shifts that may be relevant for soil functioning and could serve as  
696 indicators of potential soil health deterioration.

697 This has direct implications for long-term monitoring and remote sensing. Our model framework—by  
698 avoiding reliance on matric potential data and instead using moisture state categories and decomposed  
699 climatic features—is compatible with satellite-derived products. As remote sensing missions  
700 increasingly provide continuous global soil water content estimates, the proposed framework could be

701 adapted for large-scale assessment of soil system stability. Furthermore, under scenarios of future  
702 climate change, where shifts in precipitation patterns and evaporative demand are expected, data-driven  
703 models trained on historical data may become progressively outdated. The presented residual-based  
704 approach (quantifying MB) enables early detection of such divergence, offering a method for  
705 identifying when model retraining or reparameterization is needed to maintain predictive reliability  
706 under non-stationary conditions.

## 707 5. Summary and conclusions

708 The Temporal variations in the water content of the topsoil control near-surface hydraulic conditions,  
709 infiltration, evaporation, and gas exchange, thereby shaping soil water dynamics and physical soil  
710 functioning. Reliable information on soil water content dynamics in response to atmospheric conditions  
711 is thus essential to detect and mitigate critical changes in soil hydraulic behaviour. This response  
712 depends on soil hydraulic properties that are traditionally characterized by a time-invariant and  
713 unambiguous relationship between matric potential, water content, and hydraulic conductivity as  
714 deduced from small-scale lab experiments. In this study, we developed and applied a feed-forward  
715 neural network combined with seasonal trend analysis of climatic time series to quantify the soil water  
716 content response function after an extreme drought in summer 2018 in Germany. By analysing the time  
717 series of topsoil water content measured at two lysimeter stations of the TERENO SOILCan network,  
718 we summarize the conclusion on the soil water content response function as follows:

- 719 • 50% of the lysimeters showed changes in soil water content dynamics after the dry summer  
720 2018 without recovery until the year 2023.
- 721 • The other half showed a resilient behaviour, and the soil water content response function was  
722 not permanently changed.
- 723 • The changes in soil water content response function were manifested as (i) temporal trends in  
724 prediction error (mean bias) and (ii) shifts in the soil water characteristics function.

- 725       • The soil water content response function is adapted to climatic conditions as manifested by (i)  
726       smallest changes in lysimeters that were not translocated and (ii) decreased model performance  
727       for applications of a response function that was determined for another climate.
- 728       • Good model performance as expressed by high Nash-Sutcliffe efficiency values does not  
729       correspond to stable soil water content response function that was only detected by temporal  
730       trends in error metrics.

731 The study revealed that intense drought events can induce lasting changes in soil hydraulic properties,  
732 but the degree of resilience depends on both soil type and climatic conditions. We argue that soils which  
733 developed under a broader range of climatic conditions may possess soil hydraulic properties that  
734 enhance resilience to subsequent drought, and that this inherited behaviour persists after translocation  
735 to a new climatic regime. Because the presented model framework does (i) not aim to predict  
736 successfully time series in water content and (ii) only require categorical water content information  
737 ('stable', 'resilient', 'changed'), it can be applied to larger scale using remote sensing data that do not  
738 provide accurate soil water content values but reliable trends, enabling to detect changes in hydraulic  
739 behaviour at the ecosystem scale.

## 740       Author contributions

741 NA, AC, and PL designed the study. NA and PL conducted the research. NA developed the model and  
742 wrote the code. NA and PL prepared the manuscript with contributions of all co-authors. JG and RG  
743 provided and quality-controlled the lysimeter data.

## 744       Acknowledgements

745 We acknowledge the support of TERENO and SOILCan, which were funded by the Helmholtz  
746 Association (HGF) and the Federal Ministry of Education and Research (BMBF, Germany).

747 We would like to thank Ines Merbach, Sylvia Schmögner, Werner Küpper, Philipp Meulendick,  
748 Ferdinand Engels, Antonio Voss, Leander Fürst and Rainer Harms for their kind support at the lysimeter

749 stations in Bad Lauchstädt and Selhausen. We thank Hans-Jörg Vogel for his constructive feedback and  
750 insightful comments on the manuscript.

## 751 Financial support

752 This research is part of the project AI4SoilHealth of the European Union's Horizon research and  
753 innovation programme (grant agreement No. 101086179). This work has received funding from the  
754 Swiss State Secretariat for Education, Research and Innovation (SERI).

## 755 References

756 Allen, R. G., Pereira, L. S., Raes, D., and Smith, M.: Crop evapotranspiration – Guidelines for  
757 computing crop water requirements, FAO Irrigation and Drainage Paper 56, Food and  
758 Agriculture Organization of the United Nations, Rome, 300 pp., 2006.

759 Aqel, N., Reusser, L., Margreth, S., Carminati, A., and Lehmann, P.: Prediction of hysteretic  
760 matric potential dynamics using artificial intelligence: application of autoencoder neural  
761 networks, *Geosci. Model Dev.*, 17, 6949–6966, <https://doi.org/10.5194/gmd-17-6949-2024>,  
762 2024.

763 Blöschl, G., Bierkens, M. F. P., Chambel, A., Cudennec, C., Destouni, G., Fiori, A., Kirchner, J. W.,  
764 McDonnell, J. J., Savenije, H. H. G., Sivapalan, M., Stumpp, C., Toth, E., Volpi, E., Carr, G.,  
765 Lupton, C., Salinas, J., Széles, B., Viglione, A., Aksoy, H., and Zhang, Y.: Twenty-three unsolved  
766 problems in hydrology (UPH) – a community perspective, *Hydrol. Sci. J.*, 64, 1141–1158,  
767 <https://doi.org/10.1080/02626667.2019.1620507>, 2019.

768 Boergens, E., Güntner, A., Sips, M., Schwatke, C., and Dobsław, H.: Interannual variations of  
769 terrestrial water storage in the East African Rift region, *Hydrol. Earth Syst. Sci.*, 28, 4733–4754,  
770 <https://doi.org/10.5194/hess-28-4733-2024>, 2024.

771 Bogena, H. R., Huisman, J. A., Güntner, A., Hübner, C., Kusche, J., Jonard, F., Vey, S., and  
772 Vereecken, H.: Emerging methods for noninvasive sensing of soil moisture dynamics from field  
773 to catchment scale: a review, *WIREs Water*, 2, 635–647, <https://doi.org/10.1002/wat2.1097>,  
774 2015.

775 Brocca, L., Melone, F., Moramarco, T., Wagner, W., Naeimi, V., Bartalis, Z., and Hasenauer, S.:  
776 Improving runoff prediction through the assimilation of the ASCAT soil moisture product,  
777 *Hydrol. Earth Syst. Sci.*, 14, 1881–1893, <https://doi.org/10.5194/hess-14-1881-2010>, 2010.

778 Cleveland, R. B., Cleveland, W. S., McRae, J. E., and Terpenning, I.: STL: A seasonal-trend  
779 decomposition procedure based on Loess, *J. Off. Stat.*, 6, 3–73, 1990.

780 Detty, J. M. and McGuire, K. J.: Threshold changes in storm runoff generation at a till-mantled  
781 headwater catchment, *Water Resour. Res.*, 46, W07525,  
782 <https://doi.org/10.1029/2009WR008102>, 2010.

783 Deutscher Wetterdienst (DWD) Climate Data Center (CDC): Historical daily precipitation data,  
784 station Leipzig/Halle (ID 2932), available at: <https://www.dwd.de/cdc> (last access: 28 August  
785 2025), 2025.

786 Fatichi, S., Or, D., Walko, R., Vereecken, H., Young, M. H., Ghezzehei, T. A., Hengl, T., Kollet, S.,  
787 Agam, N., and Avissar, R.: Soil structure is an important omission in Earth system models, *Nat.*  
788 *Commun.*, 11, 522, <https://doi.org/10.1038/s41467-020-14411-z>, 2020.

789 Fu, Z., Hu, W., Beare, M., Thomas, S., Carrick, S., Dando, J., Langer, S., Müller, K., Baird, D., and  
790 Lilburne, L.: Land use effects on soil hydraulic properties and the contribution of soil organic  
791 carbon, *J. Hydrol.*, 602, 126741, <https://doi.org/10.1016/j.jhydrol.2021.126741>, 2021.

792 Groh, J., Diamantopoulos, E., Duan, X., Ewert, F., Heinlein, F., Herbst, M., Holbak, M., Kamali, B.,  
793 Kersebaum, K.-C., Kuhnert, M., Nendel, C., Priesack, E., Steidl, J., Sommer, M., Pütz, T.,  
794 Vanderborght, J., Vereecken, H., Wallor, E., Weber, T. K. D., and Gerke, H. H.: Same soil,  
795 different climate: crop model intercomparison on translocated lysimeters, *Vadose Zone J.*, 21,  
796 e20202, <https://doi.org/10.1002/vzj2.20202>, 2022.

797 Groh, J., Vanderborght, J., Pütz, T., Vogel, H.-J., Gründling, R., Rupp, H., Rahmati, M., Sommer,  
798 M., Vereecken, H., and Gerke, H. H.: Responses of soil water storage and crop water use  
799 efficiency to changing climatic conditions: a lysimeter-based space-for-time approach, *Hydrol.*  
800 *Earth Syst. Sci.*, 24, 1211–1225, <https://doi.org/10.5194/hess-24-1211-2020>, 2020.

801 Hannes, M., Wollschläger, U., Wöhling, T., and Vogel, H.-J.: Revisiting hydraulic hysteresis based  
802 on long-term monitoring of hydraulic states in lysimeters, *Water Resour. Res.*, 52, 3847–3865,  
803 <https://doi.org/10.1002/2015WR018319>, 2016.

804 Hari, V., Rakovec, O., Markonis, Y., Hanel, M., and Kumar, R.: Increased future occurrences of  
805 the exceptional 2018–2019 Central European drought under global warming, *Sci. Rep.*, 10,  
806 12207, <https://doi.org/10.1038/s41598-020-68872-9>, 2020.

807 Herbrich, M. and Gerke, H. H.: Scales of water retention dynamics observed in eroded Luvisols  
808 from an arable postglacial soil landscape, *Vadose Zone J.*, 16, 1–12,  
809 <https://doi.org/10.2136/vzj2017.01.0003>, 2017.

810 Hirmas, D. R., Giménez, D., Nemes, A., Kerry, R., Brunsell, N. A., and Wilson, C. J.: Climate-  
811 induced changes in continental-scale soil macroporosity may intensify water cycle, *Nature*, 561,  
812 100–103, <https://doi.org/10.1038/s41586-018-0463-x>, 2018.

813 Holling, C. S.: Resilience and stability of ecological systems, IIASA Research Report RR-73-003  
814 (Reprint), IIASA, Laxenburg, Austria, reprinted from *Annual Review of Ecology and Systematics*,  
815 4, 1–23, <https://pure.iiasa.ac.at/id/eprint/26/1/RP-73-003.pdf>, 1973.

816 Hrachowitz, M., Savenije, H. H. G., Blöschl, G., McDonnell, J. J., Sivapalan, M., Pomeroy, J. W.,  
817 Arheimer, B., Blume, T., Clark, M. P., Ehret, U., Fenicia, F., Freer, J. E., Gelfan, A., Gupta, H. V.,  
818 Hughes, D. A., Hut, R. W., Montanari, A., Pande, S., Tetzlaff, D., and Cudennec, C.: A decade of  
819 Predictions in Ungauged Basins (PUB) – a review, *Hydrol. Sci. J.*, 58, 1198–1255,  
820 <https://doi.org/10.1080/02626667.2013.803183>, 2013.

821 Jarvis, N. J., Coucheney, E., Lewan, E., Klöffel, T., Meurer, K. H. E., Keller, T., and Larsbo, M.:  
822 Interactions between soil structure dynamics, hydrological processes and organic matter  
823 cycling: a new soil-crop model, *Eur. J. Soil Sci.*, 75, e13455, <https://doi.org/10.1111/ejss.13455>,  
824 2024.

825 Kingma, D. P., and Ba, J.: Adam: A method for stochastic optimization, Proceedings of the  
826 International Conference on Learning Representations (ICLR), 2015,  
827 <https://arxiv.org/abs/1412.6980>, 2015.

828 Klöffel, T., Barron, J., Nemes, A., Giménez, D., and Jarvis, N. J.: Soil, climate, time and site  
829 factors as drivers of soil structure evolution in agricultural soils from a temperate-boreal  
830 region, *Geoderma*, 442, 116772, <https://doi.org/10.1016/j.geoderma.2024.116772>, 2024.

831 Kratzert, F., Klotz, D., Shalev, G., Klambauer, G., Hochreiter, S., and Nearing, G. S.: Towards  
832 learning universal, regional, and local hydrological behaviours via machine learning applied to  
833 large-sample datasets, *Hydrol. Earth Syst. Sci.*, 23, 5089–5110, [https://doi.org/10.5194/hess-](https://doi.org/10.5194/hess-23-5089-2019)  
834 [23-5089-2019](https://doi.org/10.5194/hess-23-5089-2019), 2019.

835 Kuzyakov, Y., and Zamanian, K.: Reviews and syntheses: Agropedogenesis – humankind as the  
836 sixth soil-forming factor and attractors of agricultural soil degradation, *Biogeosciences*, 16,  
837 4783–4803, <https://doi.org/10.5194/bg-16-4783-2019>, 2019.

838 Lehmann, P., Bickel, S., Wei, Z., and Or, D.: Physical constraints for improved soil hydraulic  
839 parameter estimation by pedotransfer functions, *Water Resour. Res.*, 56, e2019WR025963,  
840 <https://doi.org/10.1029/2019WR025963>, 2020.

841 Liu, J., Hughes, D., Rahmani, F., Lawson, K., and Shen, C.: Evaluating a global soil moisture  
842 dataset from a multitask model (GSM3 v1.0) with potential applications for crop threats,  
843 *Geosci. Model Dev.*, 16, 1553–1567, <https://doi.org/10.5194/gmd-16-1553-2023>, 2023.

844 Liu, J., Rahmani, F., Lawson, K., and Shen, C.: A multiscale deep learning model for soil moisture  
845 integrating satellite and in situ data, *Geophys. Res. Lett.*, 49, e2021GL096847,  
846 <https://doi.org/10.1029/2021GL096847>, 2022.

847 Liu, Y. Y., Parinussa, R. M., Dorigo, W. A., De Jeu, R. A. M., Wagner, W., van Dijk, A. I. J. M.,  
848 McCabe, M. F., and Evans, J. P.: Developing an improved soil moisture dataset by blending  
849 passive and active microwave satellite-based retrievals, *Hydrol. Earth Syst. Sci.*, 15, 425–436,  
850 <https://doi.org/10.5194/hess-15-425-2011>, 2011.

851 Lu, L., Shin, Y., Su, Y., and Karniadakis, G. E.: Dying ReLU and initialization: theory and numerical  
852 examples, *Commun. Comput. Phys.*, 28, 1671–1706, [https://doi.org/10.4208/cicp.OA-2020-](https://doi.org/10.4208/cicp.OA-2020-0165)  
853 [0165](https://doi.org/10.4208/cicp.OA-2020-0165), 2020.

854 Melsen, L. A. and Guse, B.: Climate change impacts model parameter sensitivity – implications  
855 for calibration strategy and model diagnostic evaluation, *Hydrol. Earth Syst. Sci.*, 25, 1307–  
856 1332, <https://doi.org/10.5194/hess-25-1307-2021>, 2021.

857 Milly, P. C. D., Betancourt, J., Falkenmark, M., Hirsch, R. M., Kundzewicz, Z. W., Lettenmaier, D.  
858 P., and Stouffer, R. J.: Stationarity is dead: whither water management?, *Science*, 319, 573–  
859 574, <https://doi.org/10.1126/science.1151915>, 2008.

860 Montanari, A., Young, G., Savenije, H. H. G., Hughes, D., Wagener, T., Ren, L.-L., Koutsoyiannis,  
861 D., Cudennec, C., Toth, E., Grimaldi, S., Blöschl, G., Sivapalan, M., Beven, K., Gupta, H., Hipsey,  
862 B., Schaeffli, B., Arheimer, B., Boegh, E., Schymanski, S. J., and Belyaev, V.: “Panta Rhei—  
863 Everything Flows”: change in hydrology and society—The IAHS Scientific Decade 2013–2022,  
864 *Hydrol. Sci. J.*, 58, 1256–1275, <https://doi.org/10.1080/02626667.2013.809088>, 2013.

865 Montesinos López, O. A., Montesinos López, A., and Crossa, J.: Fundamentals of artificial neural  
866 networks and deep learning, in: *Multivariate Statistical Machine Learning Methods for*  
867 *Genomic Prediction*, Springer International Publishing, Cham, 379–425,  
868 [https://doi.org/10.1007/978-3-030-89010-0\\_10](https://doi.org/10.1007/978-3-030-89010-0_10), 2022.

869 Moriasi, D. N., Arnold, J. G., Van Liew, M. W., Bingner, R. L., Harmel, R. D., and Veith, T. L.:  
870 Model evaluation guidelines for systematic quantification of accuracy in watershed  
871 simulations, *Trans. ASABE*, 50, 885–900, <https://doi.org/10.13031/2013.23153>, 2007.

872 Moriasi, D. N., Gitau, M. W., Pai, N., and Daggupati, P.: Hydrologic and water quality models:  
873 Performance measures and evaluation criteria, *Trans. ASABE*, 58, 1763–1785, 2015.  
874 <https://web.ics.purdue.edu/~mgitau/pdf/Moriasi%20et%20al%202015.pdf>

875 Mosavi, A., Ozturk, P., and Chau, K.-W.: Flood prediction using machine learning models:  
876 literature review, *Water*, 10, 1536, <https://doi.org/10.3390/w10111536>, 2018.

877 Nash, J. E. and Sutcliffe, J. V.: River flow forecasting through conceptual models part I — A  
878 discussion of principles, *J. Hydrol.*, 10, 282–290, [https://doi.org/10.1016/0022-1694\(70\)90255-](https://doi.org/10.1016/0022-1694(70)90255-6)  
879 6, 1970.

880 Nearing, G. S., Kratzert, F., Sampson, A. K., Pelissier, C. S., Klotz, D., Frame, J. M., Prieto, C., and  
881 Gupta, H. V.: What role does hydrological science play in the age of machine learning?, *Water*  
882 *Resour. Res.*, 57, e2020WR028091, <https://doi.org/10.1029/2020WR028091>, 2021.

883 O., S. and Orth, R.: Global soil moisture data derived through machine learning trained with in-  
884 situ measurements, *Sci. Data*, 8, 170, <https://doi.org/10.1038/s41597-021-00964-1>, 2021.

885 Pütz, T., Kiese, R., Wollschläger, U., Groh, J., Rupp, H., Zacharias, S., Priesack, E., Gerke, H. H.,  
886 Gasche, R., Bens, O., Borg, E., Baessler, C., Kaiser, K., Herbrich, M., Munch, J.-C., Sommer, M.,  
887 Vogel, H.-J., Vanderborght, J., and Vereecken, H.: TERENO-SOILCan: a lysimeter-network in  
888 Germany observing soil processes and plant diversity influenced by climate change, *Environ.*  
889 *Earth Sci.*, 75, 1242, <https://doi.org/10.1007/s12665-016-6031-5>, 2016.

890 Quintana, J. R., Martín-Sanz, J. P., Valverde-Asenjo, I., and Molina, J. A.: Drought differently  
891 destabilizes soil structure in a chronosequence of abandoned agricultural lands, *Catena*, 222,  
892 106871, <https://doi.org/10.1016/j.catena.2022.106871>, 2023.

893 Reichstein, M., Camps-Valls, G., Stevens, B., Jung, M., Denzler, J., Carvalhais, N., and Prabhat:  
894 Deep learning and process understanding for data-driven Earth system science, *Nature*, 566,  
895 195–204, <https://doi.org/10.1038/s41586-019-0912-1>, 2019.

896 Robinson, D. A., Jones, S. B., Lebron, I., Reinsch, S., Domínguez, M. T., Smith, A. R., Jones, D. L.,  
897 Marshall, M. R., and Emmett, B. A.: Experimental evidence for drought induced alternative  
898 stable states of soil moisture, *Sci. Rep.*, 6, 20018, <https://doi.org/10.1038/srep20018>, 2016.

899 Robinson, D. A., Hopmans, J. W., Filipović, V., van der Ploeg, M., Lebron, I., Jones, S. B., Reinsch,  
900 S., Jarvis, N., and Tuller, M.: Global environmental changes impact soil hydraulic functions  
901 through biophysical feedbacks, *Glob. Change Biol.*, 25, 1895–1904,  
902 <https://doi.org/10.1111/gcb.14626>, 2019.

903 Robinson, D. A., Nemes, A., Reinsch, S., Radbourne, A., Bentley, L., and Keith, A. M.: Global  
904 meta-analysis of soil hydraulic properties on the same soils with differing land use, *Sci. Total*  
905 *Environ.*, 852, 158506, <https://doi.org/10.1016/j.scitotenv.2022.158506>, 2022.

906 Sainju, U. M., Liptzin, D., and Jabro, J. D.: Relating soil physical properties to other soil  
907 properties and crop yields, *Sci. Rep.*, 12, 22025, <https://doi.org/10.1038/s41598-022-26619-8>,  
908 2022.

909 Seneviratne, S. I., Corti, T., Davin, E. L., Hirschi, M., Jaeger, E. B., Lehner, I., Orlowsky, B., and  
910 Teuling, A. J.: Investigating soil moisture–climate interactions in a changing climate: a review,  
911 *Earth-Sci. Rev.*, 99, 125–161, <https://doi.org/10.1016/j.earscirev.2010.02.004>, 2010.

912 Shen, C., Laloy, E., Elshorbagy, A., Albert, A., Bales, J., Chang, F.-J., Ganguly, S., Hsu, K.-L., Kifer,  
913 D., Fang, Z., Fang, K., Li, D., Li, X., and Tsai, W.-P.: HESS Opinions: Incubating deep-learning-  
914 powered hydrologic science advances as a community, *Hydrol. Earth Syst. Sci.*, 22, 5639–5656,  
915 <https://doi.org/10.5194/hess-22-5639-2018>, 2018.

916 Sun, W., Zhou, S., Yu, B., Zhang, Y., Keenan, T., and Fu, B.: Soil moisture–atmosphere  
917 interactions drive terrestrial carbon–water trade-offs, *Commun. Earth Environ.*, 6, 169,  
918 <https://doi.org/10.1038/s43247-025-02145-z>, 2025.

919 Tromp-van Meerveld, H. J. and McDonnell, J. J.: Threshold relations in subsurface stormflow: 1.  
920 A 147-storm analysis of the Panola hillslope, *Water Resour. Res.*, 42, W02410,  
921 <https://doi.org/10.1029/2004WR003778>, 2006.

922 Uber, M., Vandervaere, J.-P., Zin, I., Braud, I., Heistermann, M., Legoût, C., Molinié, G., and  
923 Nord, G.: How does initial soil moisture influence the hydrological response? A case study from  
924 southern France, *Hydrol. Earth Syst. Sci.*, 22, 6127–6146, [https://doi.org/10.5194/hess-22-](https://doi.org/10.5194/hess-22-6127-2018)  
925 6127-2018, 2018.

926 Vaze, J., Post, D. A., Chiew, F. H. S., Perraud, J.-M., Viney, N. R., and Teng, J.: Climate non-  
927 stationarity – validity of calibrated rainfall–runoff models for use in climate change studies, *J.*  
928 *Hydrol.*, 394, 447–457, <https://doi.org/10.1016/j.jhydrol.2010.09.018>, 2010.

929 Vereecken, H., Amelung, W., Bauke, S. L., Boga, H., Brüggemann, N., Montzka, C.,  
930 Vanderborght, J., Bechtold, M., Blöschl, G., Carminati, A., Javaux, M., Konings, A. G., Kusche, J.,  
931 Neuweiler, I., Or, D., Steele-Dunne, S., Verhoef, A., Young, M., and Zhang, Y.: Soil hydrology in  
932 the Earth system, *Nat. Rev. Earth Environ.*, 3, 573–587, [https://doi.org/10.1038/s43017-022-](https://doi.org/10.1038/s43017-022-00324-6)  
933 00324-6, 2022.

934 Vereecken, H., Huisman, J. A., Boga, H., Vanderborght, J., Vrugt, J. A., and Hopmans, J. W.:  
935 On the value of soil moisture measurements in vadose zone hydrology: a review, *Water*  
936 *Resour. Res.*, 44, W00D06, <https://doi.org/10.1029/2008WR006829>, 2008.

937 Wankmüller, F. J. P., Delval, L., Lehmann, P., Baur, M. J., Cecere, A., Wolf, S., Or, D., Javaux, M.,  
938 and Carminati, A.: Global influence of soil texture on ecosystem water limitation, *Nature*, 635,  
939 631–638, <https://doi.org/10.1038/s41586-024-08089-2>, 2024.

940 Western, A. W. and Grayson, R. B.: The Tarrawarra data set: soil moisture patterns, soil  
941 characteristics, and hydrological flux measurements, *Water Resour. Res.*, 34, 2765–2768,  
942 <https://doi.org/10.1029/98WR01833>, 1998.

943 Xoplaki, E., Ellsäßer, F., Grieger, J., Nissen, K. M., Pinto, J. G., Augenstein, M., Chen, T.-C., and  
944 Wolf, F.: Compound events in Germany in 2018: drivers and case studies, *Nat. Hazards Earth*  
945 *Syst. Sci.*, 25, 541–564, <https://doi.org/10.5194/nhess-25-541-2025>, 2025.

- 946 Zehe, E. and Blöschl, G.: Predictability of hydrologic response at the plot and catchment scales:  
947 role of initial conditions, *Water Resour. Res.*, 40, W10240,  
948 <https://doi.org/10.1029/2003WR002869>, 2004.
- 949 Šimůnek, J., van Genuchten, M. T., and Šejna, M.: Recent developments and applications of the  
950 HYDRUS computer software packages, *Vadose Zone J.*, 15, 1–25,  
951 <https://doi.org/10.2136/vzj2016.04.0033>, 2016.